

HUBBLE SPACE TELESCOPE NEAR-ULTRAVIOLET SPECTROSCOPY OF THE BRIGHT CEMP-NO STAR BD+44°493¹

VINICIUS M. PLACCO², TIMOTHY C. BEERS^{3,4}, IAN U. ROEDERER⁵, JOHN J. COWAN⁶, ANNA FREBEL⁷,
DAN FILLER⁸, INESE I. IVANS⁸, JAMES E. LAWLER⁹, HENDRIK SCHATZ^{4,10}, CHRISTOPHER SNEDEN¹¹,
JENNIFER S. SOBECK¹², WAKO AOKI¹³, VERNE V. SMITH³

(Received April 11, 2014; Accepted June 2, 2014)
Draft version January 30, 2018

ABSTRACT

We present an elemental-abundance analysis, in the near-ultraviolet (NUV) spectral range, for the extremely metal-poor star BD+44°493, a 9th magnitude subgiant with $[\text{Fe}/\text{H}] = -3.8$ and enhanced carbon, based on data acquired with the Space Telescope Imaging Spectrograph on the *Hubble Space Telescope*. This star is the brightest example of a class of objects that, unlike the great majority of carbon-enhanced metal-poor (CEMP) stars, does not exhibit over-abundances of heavy neutron-capture elements (CEMP-no). In this paper, we validate the abundance determinations for a number of species that were previously studied in the optical region, and obtain strong upper limits for beryllium and boron, as well as for neutron-capture elements from zirconium to platinum, many of which are not accessible from ground-based spectra. The boron upper limit we obtain for BD+44°493, $\log \epsilon(\text{B}) < -0.70$, the first such measurement for a CEMP star, is the lowest yet found for very and extremely metal-poor stars. In addition, we obtain even lower upper limits on the abundances of beryllium, $\log \epsilon(\text{Be}) < -2.3$, and lead, $\log \epsilon(\text{Pb}) < -0.23$ ($[\text{Pb}/\text{Fe}] < +1.90$), than those reported by previous analyses in the optical range. Taken together with the previously measured low abundance of lithium, the very low upper limits on Be and B suggest that BD+44°493 was formed at a very early time, and that it could well be a bona-fide second-generation star. Finally, the Pb upper limit strengthens the argument for non-*s*-process production of the heavy-element abundance patterns in CEMP-no stars.

Subject headings: Galaxy: halo—techniques: spectroscopy—stars: abundances—stars: atmospheres—stars: Population II—stars: individual (BD+44°493)

1. INTRODUCTION

Carbon-enhanced metal-poor (CEMP) stars are a subset of metal-poor (MP; $[\text{Fe}/\text{H}]^{14} < -1.0$, e.g., [Beers &](#)

[Christlieb 2005](#); [Frebel & Norris 2013](#)) and very metal-poor (VMP; $[\text{Fe}/\text{H}] < -2.0$) stars that exhibit elevated carbon relative to iron, $[\text{C}/\text{Fe}]$, sometimes referred to as carbonicity ($[\text{C}/\text{Fe}] \geq +1.0$; [Placco et al. 2011](#)). It has recently been recognized that a more appropriate division on $[\text{C}/\text{Fe}]$ for the identification of CEMP stars is at somewhat lower carbonicity, e.g., $[\text{C}/\text{Fe}] \geq +0.7$ ([Aoki et al. 2007](#); [Carollo et al. 2012](#); [Norris et al. 2013](#)). In the past few decades, it has become clear that such stars comprise a significant fraction of all VMP stars (~ 10 -20%; [Beers et al. 1992](#); [Norris et al. 1997](#); [Rossi et al. 1999](#); [Beers & Christlieb 2005](#); [Cohen et al. 2005](#); [Marsteller et al. 2005](#); [Rossi et al. 2005](#); [Frebel et al. 2006b](#); [Lucatello et al. 2006](#); [Norris et al. 2007](#); [Carollo et al. 2012](#); [Cohen et al. 2013](#); [Norris et al. 2013](#); [Spite et al. 2013](#)), one that increases strongly with declining metallicity, from 30% for $[\text{Fe}/\text{H}] < -3.0$, to 40% for $[\text{Fe}/\text{H}] < -3.5$, $\sim 75\%$ for $[\text{Fe}/\text{H}] < -4.0$ and 100% for $[\text{Fe}/\text{H}] < -5.0$. This trend has been confirmed with the many thousands of CEMP stars identified by [Lee et al. \(2013\)](#) from the Sloan Digital Sky Survey (SDSS; [York et al. 2000](#)), and its extensions SEGUE-1 (Sloan Extension for Galactic Exploration and Understanding; [Yanny et al. 2009](#)) and SEGUE-2 (C. Rockosi et al., in preparation).

For most CEMP stars there exists a clear correlation between carbon enhancement and the over-abundance of elements produced by *s*-process nucleosynthesis, such as Ba (CEMP-*s* stars; see [Beers & Christlieb 2005](#)). This behavior is consistent with the hypothesis that these enhancements (both for carbon and elements produced by

¹ Based on observations made with the NASA/ESA Hubble Space Telescope, obtained at the Space Telescope Science Institute, which is operated by the Association of Universities for Research in Astronomy, Inc., under NASA contract NAS 5-26555. These observations are associated with program GO-12554, and we also make use of data taken in program GO-12268.

² Gemini Observatory, Hilo, HI 96720, USA

³ National Optical Astronomy Observatory, Tucson, AZ 85719, USA

⁴ JINA: Joint Institute for Nuclear Astrophysics

⁵ Department of Astronomy, University of Michigan, Ann Arbor, MI 48109, USA

⁶ Homer L. Dodge Department of Physics and Astronomy, University of Oklahoma, Norman, OK 73019, USA

⁷ Kavli Institute for Astrophysics and Space Research and Department of Physics, Massachusetts Institute of Technology, Cambridge, MA 02139, USA

⁸ Department of Physics and Astronomy, The University of Utah, Salt Lake City, UT 84112, USA

⁹ Department of Physics, University of Wisconsin, Madison, WI 53706, USA

¹⁰ National Superconducting Cyclotron Laboratory, Michigan State University, East Lansing, MI 48824, USA

¹¹ Department of Astronomy and McDonald Observatory, University of Texas, Austin, TX 78712, USA

¹² Department of Astronomy, University of Virginia, Charlottesville, VA 22904, USA

¹³ National Astronomical Observatory of Japan, 2-21-1 Osawa, Mitaka, Tokyo 181-8588, Japan

¹⁴ $[\text{A}/\text{B}] = \log(N_{\text{A}}/N_{\text{B}})_{\star} - \log(N_{\text{A}}/N_{\text{B}})_{\odot}$, where N is the number density of atoms of a given element, and the indices refer to the star (\star) and the Sun (\odot).

the *s*-process) are due to nucleosynthesis processes that took place during the asymptotic giant-branch (AGB) stage of stellar evolution (e.g., Herwig 2005; Sneden et al. 2008). The resulting abundance pattern can arise from the star itself (which should rarely be found, but see Masseron et al. 2006) or by a now-extinct binary companion that transferred material to the surviving (observed) companion (Stancliffe & Glebbeek 2008). Multi-epoch radial-velocity measurements by McClure (1983), McClure & Woodsworth (1990), and Jorissen et al. (1998) demonstrated that the frequency of detected binaries among equivalent Population I Ba stars and Population II CH stars indicated that essentially all are members of binary systems. Lucatello et al. (2005) conducted a similar study for members of the more metal-deficient CEMP-*s* sub-class of stars, and reached the same conclusion.

An intriguing variation on this behavior was initially recognized by Barbuy et al. (1997) and Hill et al. (2000). The CEMP stars CS 22948-027 and CS 29497-034 were found not only to be rich in the elements commonly produced by *s*-process nucleosynthesis, such as Sr, Y, Ba, and La, but also in Eu, an element that, for extremely low-metallicity stars, is more likely produced by *r*-process nucleosynthesis. Additional studies by many groups have now identified ~ 50 of these so-called CEMP-*r/s* stars. These cases, once thought to be the rare exceptions, are as commonly represented among CEMP stars as the “*s*-only” variety. The origin of the abundance patterns of the CEMP-*r/s* stars is not yet clear, and many scenarios have been proposed (Jonsell et al. 2006; Masseron et al. 2010; Lugaro et al. 2012). For example, an association with a ^{22}Ne neutron source in intermediate-mass AGB stars has been suggested for progenitors of CEMP-*r/s* stars, rather than the ^{13}C neutron source thought to be active for low-mass AGB stars, the likely progenitors of the CEMP-*s* stars (Placco et al. 2013, Hollek et al. 2014, submitted). Mass transfer from a companion that passed through the AGB phase of stellar evolution has been suggested previously as an explanation for the CEMP-*s* and CEMP-*r/s* classes of stars, based on the high fraction of such stars found in binary systems (Masseron et al. 2010; Allen et al. 2012; Bisterzo et al. 2012).

The story has become richer still. Aoki et al. (2007), and others since, have shown that the correlation between carbon enhancement and the over-abundances of *s*- or *r/s*-elements no longer persists (or at least is different in nature) for the majority of CEMP stars with $[\text{Fe}/\text{H}] < -2.7$. These so-called CEMP-no stars (indicating no enhancement of neutron-capture elements) suggest that a variety of carbon-producing mechanisms, other than that associated with AGB stars, may have played a role in the early universe. Possible progenitors for this sub-class include massive, rapidly rotating, mega metal-poor (MMP; $[\text{Fe}/\text{H}] < -6.0$) stars, sometimes referred to as “spinstars” (Chiappini 2013), which models suggest have greatly enhanced abundances of CNO due to distinctive internal burning and mixing episodes, followed by strong mass loss (Meynet et al. 2006, 2010; Hirschi 2007). Another possible scenario is pollution of the ISM by so-called faint supernovae associated with the first generations of stars, which experience exten-

sive mixing and fallback during their explosions (Umeda & Nomoto 2005; Tominaga et al. 2007). Although more data are desired for CEMP-no stars, Hansen et al. (2013) report that the fraction of binaries among stars within this sub-class is no higher than expected for random samples of VMP giants. Cohen et al. (2013), Norris et al. (2013), Starkenburg et al. (2014), and J. Andersen et al. (in preparation) reach similar conclusions. Thus, contribution of material from an evolved binary companion is apparently not required in order to form CEMP-no stars.

The recently reported extremely metal-poor Damped Lyman- α system by Cooke et al. (2011) ($[\text{Fe}/\text{H}] \sim -3.0$) exhibits enhanced carbon ($[\text{C}/\text{Fe}] = +1.5$) and other elemental abundance signatures that Kobayashi et al. (2011b) also associate with production by faint supernovae. This observation is suggestive of similar carbon-production and enrichment mechanisms in the early universe – both locally and in high-redshift systems. It is presumably no coincidence (Beers & Christlieb 2005; Frebel et al. 2007) that five of the six stars known with $[\text{Fe}/\text{H}] < -4.5$ are confirmed CEMP-no stars (Christlieb et al. 2002; Frebel et al. 2005; Norris et al. 2007; Caffau et al. 2011; Hansen et al. 2014; Keller et al. 2014).

There are two observational keys required to advance our understanding of these ancient stars and how they are related to early Galactic chemical evolution. One is to obtain the full set of C, N, and O abundances for as many CEMP stars as possible, an activity that is being pursued by a number of groups (see, e.g., Kennedy et al. 2011; Placco et al. 2013, 2014; Roederer et al. 2014b; C. Hansen et al., in preparation; C. Kennedy et al., in preparation). The other is to obtain as complete an inventory as possible of the light and heavy neutron-capture elements for representative examples of the known varieties of CEMP stars. Although we have partial information from previous ground-based high-resolution spectroscopic observations, there remain many key elements, such as the light species Ge and Zr, and heavier species such as Os and Pt, that can only be obtained through near-ultraviolet (NUV) spectroscopy (e.g., Sneden et al. 1998; Cowan et al. 2005). The element Pb is of particular importance, as it may provide a useful discriminant between a number of possible nucleosynthesis pathways (Busso et al. 1999; Cohen et al. 2006; Ito et al. 2013).

Since it was installed on board the *Hubble Space Telescope* (*HST*) in 1997, the Space Telescope Imaging Spectrograph (STIS) has been the only instrument available for the high-resolution NUV spectroscopy required to make these measurements. We have recently completed a new *HST*/STIS observing program to collect high-quality NUV spectroscopy for three CEMP stars, including one member of each of the CEMP-no, CEMP-*s*, and CEMP-*r/s* sub-classes. In this paper, we perform an abundance analysis of high-resolution NUV spectroscopy for the star BD+44°493, the brightest known member of the sub-class of CEMP-no stars. We fill in the abundance patterns, as best as possible, for elements beyond the iron peak, including eight species not accessible from ground-based observations. Section 2 describes our observations and reductions, and compares abundances derived from NUV lines with those derived previously from optical lines by Ito et al. (2013). Section 3 describes our abundance analysis in detail. We present a brief discussion and our conclusions in Section 4.

2. OBSERVATIONS AND MEASUREMENTS

2.1. *HST/STIS Spectra*

New STIS (Kimble et al. 1998; Woodgate et al. 1998) observations of BD+44°493 were obtained as part of Program GO-12554, using the E230M echelle grating, centered on 2707 Å, and the NUV Multianode Microchannel Array detector. There were two observational sequences of four individual exposures, taken on February 28, 2012. Each sequence had an exposure time of 2 hours and 52 minutes, with a total integration time of 5 hours and 44 minutes. The $0'06 \times 0'2$ slit yields a ~ 2 -pixel resolving power ($R \equiv \lambda/\Delta\lambda$) $\sim 30,000$. Our setup produced a wavelength coverage from 2280 Å–3070 Å in a single exposure. The observations were reduced and calibrated using the standard *calstis* pipeline. The S/N of the combined spectrum varies from $\sim 50 \text{ pix}^{-1}$ near 2300 Å, to $\sim 80 \text{ pix}^{-1}$ near 2700 Å, to $>100 \text{ pix}^{-1}$ near 3070 Å.

Figure 1 shows a portion of the NUV spectra of BD+44°493, in the region of the Mg II doublet at 2800 Å. *HST/STIS* spectra of two metal-poor giants with similar atmospheric parameters are shown for comparison, HD 108317 ($T_{\text{eff}} = 5100 \text{ K}$, $[\text{Fe}/\text{H}] = -2.53$; Roederer et al. 2012b) and HD 196944 ($T_{\text{eff}} = 5170 \text{ K}$, $[\text{Fe}/\text{H}] = -2.46$; Roederer et al. 2008). The effective temperatures and surface gravities of HD 108317 and HD 196944 are comparable to BD+44°493, but their metallicities are higher by about 1.5 dex. The lower metallicity of BD+44°493 is immediately apparent from inspection of this figure. HD 108317 is moderately enhanced in *r*-process material, ($[\text{Eu}/\text{Fe}] = +0.5$; Roederer et al. 2012b), and HD 196944 is enhanced in *s*-process material ($[\text{Ba}/\text{Fe}] = +1.5$; Roederer et al. 2014a). BD+44°493 does not exhibit neutron-capture element enhancements. To better illustrate the rather striking differences, Figure 2 shows portions of the NUV spectra around the lines of several neutron-capture elements for the same three stars shown in Figure 1. Note in particular the absence of absorption by Cd I, Os II, Lu II, and Pb I for BD+44°493, which are well-known abundance markers for the operation of the *s*-process (Gallino et al. 1998; Arlandini et al. 1999; Sneden et al. 2008).

2.2. *Line Measurements*

Equivalent widths were obtained by fitting Gaussian profiles to the observed atomic lines, using the Robospect package (Waters & Hollek 2013). The line lists were based on the compilation of Roederer et al. (2012b), as well as on data retrieved from the VALD database (Kupka et al. 1999) and the National Institute of Standards and Technology Atomic Spectra Database (NIST; Kramida et al. 2013). Abundances for individual Fe I and Fe II lines, derived from equivalent widths as well as from spectral synthesis, are listed in Table 1. Figure 3 shows a sample of the NUV spectra, with a number of the Fe lines used for the synthesis.

The abundances of all Fe I and Fe II lines in our STIS spectrum were verified by spectral synthesis. We adopt the model-atmosphere parameters derived by Ito et al. (2013), $T_{\text{eff}} = 5430 \text{ K}$, $\log g = 3.4$ (cgs), $v_{\text{micro}} = 1.3 \text{ km s}^{-1}$, and $[\text{Fe}/\text{H}] = -3.8$. The iron abundances we derive from NUV lines [Fe I: $\log(\epsilon) = 3.62 \pm 0.02$; Fe II: $\log(\epsilon) = 3.63 \pm 0.02$] differ little from the values derived

by Ito et al. from optical lines [Fe I: $\log(\epsilon) = 3.67 \pm 0.01$; Fe II: $\log(\epsilon) = 3.68 \pm 0.03$].

Previous work has shown that small differences between optical and NUV Fe I and Fe II lines may exist (Roederer et al. 2010b, 2012b). For example, Figure 6 of Ito et al. reveals a small “dip” in the abundances of Fe I and Fe II lines blueward of the Balmer series limit in BD+44°493. Roederer et al. (2012b), Lawler et al. (2013), and Wood et al. (2013, 2014) investigated several causes of this effect for other metal-poor giants, but the differences are not fully understood at present. To minimize this effect, we reference abundance ratios of other elements derived from NUV transitions to the iron abundance also derived from NUV transitions.

As a check on our procedures, we also used the equivalent-width values published in Ito et al. (2013) as input to our machinery. Figure 4 shows the differences between the abundances derived by equivalent-width analysis between Ito et al. and this work. Apart from Si (which differs by -0.07 dex relative to Ito et al.), all of the other differences lie within ± 0.04 dex, with a mean difference of -0.01 dex. This test demonstrates that our analysis procedures and machinery can reproduce the Ito et al. values to excellent precision.

3. ABUNDANCE ANALYSIS AND UPPER LIMITS

Chemical abundances or upper limits were obtained from the NUV spectrum of BD+44°493 for 26 elements, including measurements for C, O, Sc, Ti, Cr, Mn, Fe, and Ni, and upper limits for Be, B, Ge, Zr, Nb, Mo, Cd, Te, Ce, Nd, Eu, Gd, Yb, Lu, Hf, Os, Pt, and Pb.

Our abundance analysis utilizes one-dimensional plane-parallel ATLAS9 model atmospheres with no over-shooting (Castelli & Kurucz 2004), computed under the assumption of local thermodynamic equilibrium (LTE). We use the 2011 version of the MOOG synthesis code (Sneden 1973) for this analysis. To treat isotropic, coherent scattering in this version of MOOG, the solution of the radiative transfer considers both absorption and scattering components, rather than treating such scattering as pure absorption (see Sobek et al. 2011, for further details).

Our final abundance ratios, $[\text{X}/\text{Fe}]$, are given with respect to the solar abundances of Asplund et al. (2009). Upper limits for elements for which no absorption lines were detected provide additional information for the interpretation of the overall abundance pattern of the stars. Based on the S/N ratio in the spectral region of the line, and employing the formula given in Frebel et al. (2006a), we derive $3\text{-}\sigma$ upper limits for 13 elements. Abundances and upper limits for individual lines, derived from both equivalent widths and spectral synthesis, are listed in Table 2.

A summary of the chemical abundances and upper limits for BD+44°493 is provided in Table 3. The σ refers to the standard error of the mean. We have also addressed the systematic uncertainties that could affect the model-atmosphere parameters. Table 4 shows the effect of changes in each atmospheric parameter on the determined abundances, using spectral lines from which abundances were determined by equivalent-width analysis alone. The adopted variations are 150 K for T_{eff} , 0.5 dex for $\log g$, and 0.3 km s^{-1} for v_{micro} . Also shown is the total uncertainty, taken as the quadratic sum of

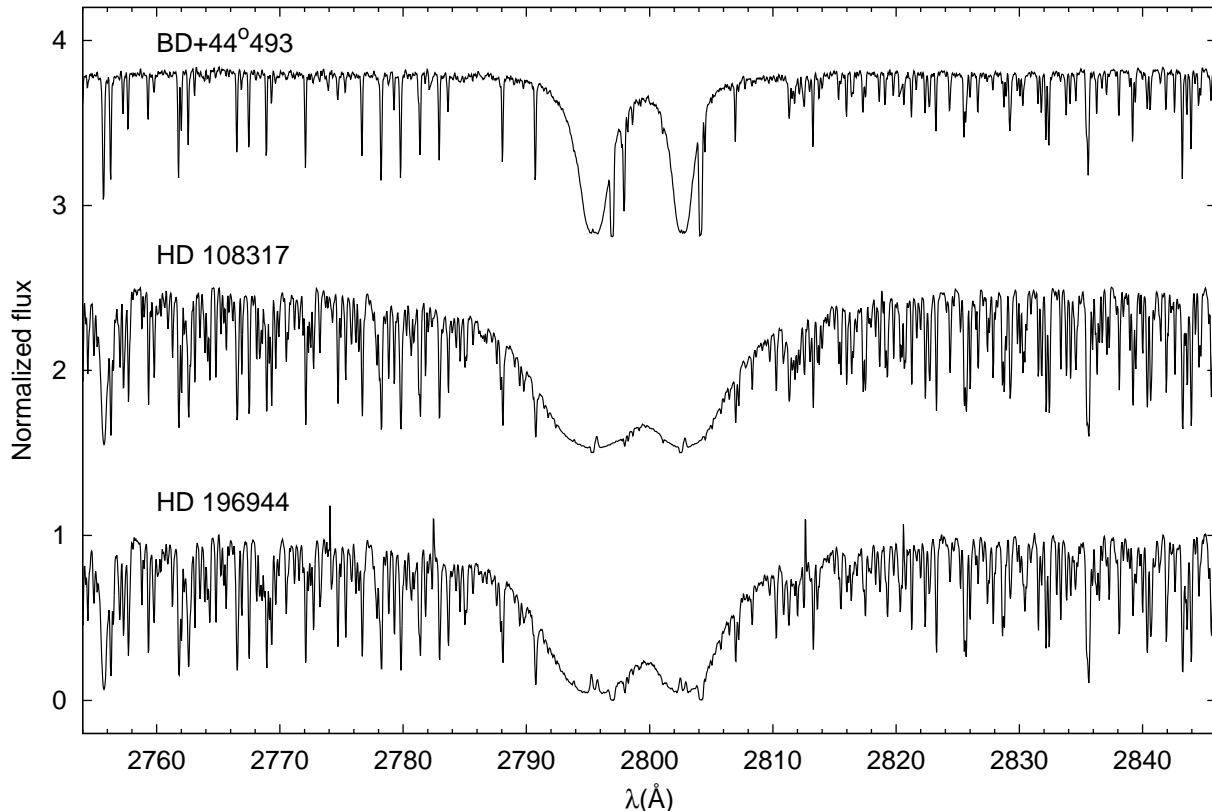


FIG. 1.— *HST*/STIS spectra for BD+44°493, HD 108317, and HD 196944, in the region of the Mg II doublet at 2800 Å. All three stars have similar T_{eff} and $\log g$; the substantially lower metallicity of BD+44°493 is immediately apparent.

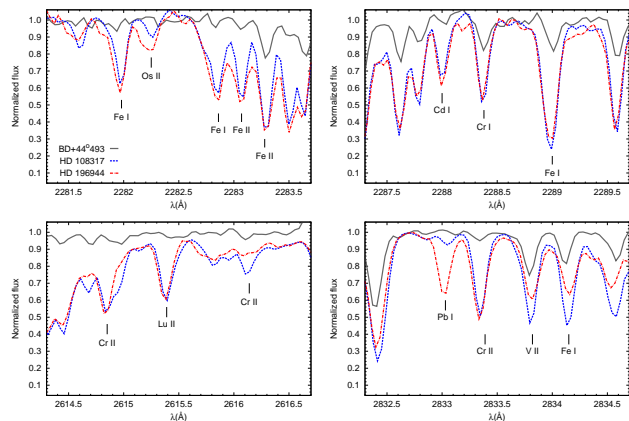


FIG. 2.— *HST*/STIS spectra for BD+44°493, HD 108317, and HD 196944, in the regions of the lines of Os II, Cd I, Lu II, and Pb I. The contrast in the abundances of these neutron-capture elements for the latter two stars, relative to BD+44°493, is clear.

the individual errors.

We discuss the determinations of beryllium, boron, carbon, the iron-peak elements, and the neutron-capture elements in more detail in the following subsections.

3.1. Beryllium and Boron

The Be I resonance line at 2348 Å is not detected in our spectrum of BD+44°493. However, we can make use of this line to place a significantly lower (by 0.5 dex, a factor of three) upper limit on the Be abundance in BD+44°493 ($\log \epsilon(\text{Be}) < -2.3$) than obtained by Ito et al. (2013) from the NUV Be II doublet at 3130 Å

($\log \epsilon(\text{Be}) < -1.8$). The blue dotted line in the left panel of Figure 5 shows our 3- σ upper limit for the Be I 2348 Å line. For comparison, the red dashed line shows the Ito et al. upper limit. We note, following Ito et al. (2013), that 3D and NLTE effects on the beryllium abundance in metal-poor stars are expected to be small (Asplund 2005).

The B I resonance doublet at 2497 Å is also not detected in our spectrum of BD+44°493. We derive an upper limit of $\log \epsilon(\text{B}) < -0.5$ from these lines, as shown in the right panel of Figure 5. NLTE corrections for measured B abundances appear to be important (e.g., Kiselman & Carlsson 1996), and could possibly perturb the results (as inferred from the NLTE calculations of Kiselman & Carlsson) by up to +0.5 dex, for stars of metallicity similar to BD+44°493. For the purpose of comparing our present upper limit on B to previous detections, we prefer to use the LTE results.

3.2. Carbon and Oxygen

The upper panels of Figure 6 show the spectral synthesis of the atomic C I features at 2478.56 Å and 2967.21 Å. Although the 2967.21 Å line is clean, the 2478 Å line is blended with several other species, and in more metal-rich stars these blends prohibit its use as an abundance indicator. The most severe of these blending features is an Fe II line at essentially the identical wavelength, 2478.57 Å. The NIST ASD database reports uncertainties of $\sigma \leq 18\%$ (≤ 0.09 dex) on the $\log gf$ values of both the C I lines. Thus, to the extent that we know the Fe abundance, and are modeling the line formation

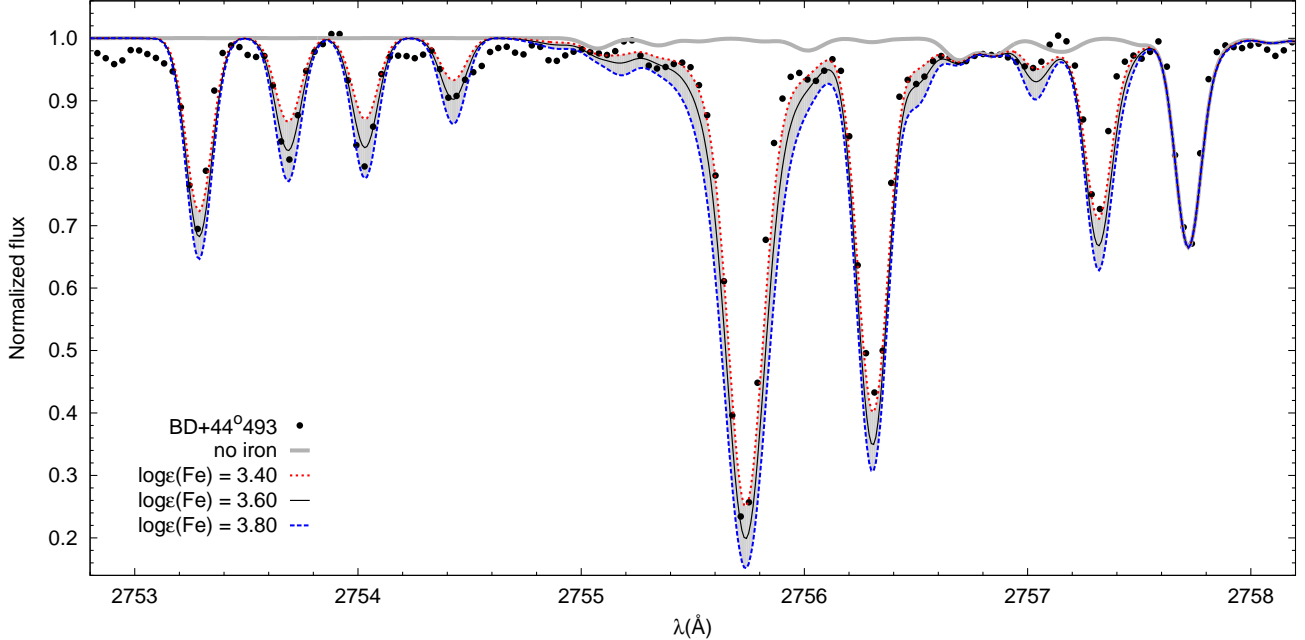


FIG. 3.— Spectral synthesis of Fe I and Fe II features. The dots represent the observed spectra, the solid line is the best abundance fit, and the dotted and dashed line are the lower and upper abundance limits, indicating the abundance uncertainty. The shaded area encompasses a 0.4 dex difference in $\log \epsilon(\text{Fe})$. The light gray line shows the synthesized spectrum in the absence of Fe.

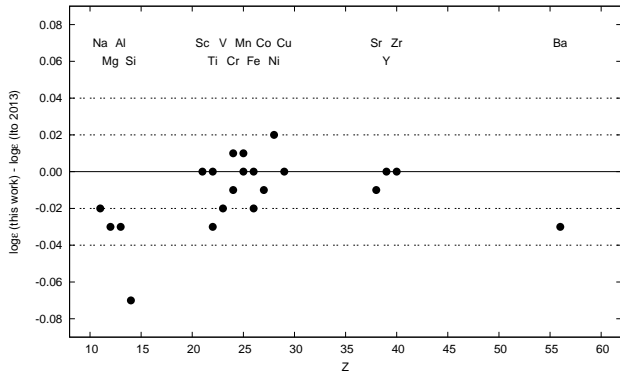


FIG. 4.— Comparison between abundances determined from the equivalent-width analysis of Ito et al. (2013) and this work. The agreement is quite satisfactory.

appropriately, we can use the C I line as a C abundance indicator in BD+44°493.

From the spectral synthesis of these lines, we obtain an average of $\log \epsilon(\text{C}) = 5.78$, which yields a carbonicity of $[\text{C}/\text{Fe}] = +1.23$ (using $[\text{Fe}/\text{H}] = -3.88$). These values agree well with the optical determinations from Ito et al. 2013 ($\log \epsilon(\text{C}) = 5.95$ and $[\text{C}/\text{Fe}] = +1.35$, using $[\text{Fe}/\text{H}] = -3.83$), but are a few tenths of a dex higher than the near-infrared (NIR) determinations from Takeda & Takada-Hidai 2013 ($\log \epsilon(\text{C}) = 5.69$ and $[\text{C}/\text{Fe}] = +0.83$, using $[\text{Fe}/\text{H}] = -3.68$). It must be kept in mind that the optical values are determined from the CH *G*-band, and the NIR from C I 1.068 – 1.069 μm lines.

To our knowledge, this is the first determination of $[\text{C}/\text{Fe}]$ based on atomic lines in the NUV region. The relatively close agreement of this determination with the $[\text{C}/\text{Fe}]$ inferred from the molecular CH *G*-band is encouraging. Previous modeling has suggested that 3D effects on the CH and C₂ features for giants and subgiants at $[\text{Fe}/\text{H}] \sim -3.0$ can lead to an over-estimate of $[\text{C}/\text{Fe}]$

of +0.5 to +0.8 dex (Asplund 2005; Collet et al. 2007), although NLTE effects are not expected to be large. Another possibility is that uncertainties in the UV opacity determination have the same magnitude as 3D effects. Schuler et al. (2008) found that the $[\text{C}/\text{Fe}]$ ratio derived from an LTE analysis of the [C I] forbidden line at 8727 Å for the CEMP star HE 1005-1429 ($[\text{Fe}/\text{H}] = -3.08$) was on the order of 0.3-0.4 dex lower than the value reported by Aoki et al. (2007), based on the molecular C₂ feature at 5170 Å. Future observations of the NUV C I features for additional (necessarily bright, and ideally extremely metal-poor) CEMP stars may thus prove illuminating.

The lower panel of Figure 6 shows the spectral region 2965 Å–2972 Å, where several OH features are available. We were able to obtain adequate fits for 11 lines with the same input abundance, using the line list from Kurucz (1993). The value of the O abundance we obtain, $[\text{O}/\text{Fe}] = +1.54$, is in good agreement with that derived by Ito et al. 2013 (also using an OH feature as an indicator), $[\text{O}/\text{Fe}] = +1.64$.

3.3. The Iron-Peak Elements

Abundances for Sc, Ti, Cr, and Ni were determined with an equivalent-width analysis only. Mn II lines are broadened by hyperfine splitting of the ⁵⁵Mn isotope, so we derived those abundances from spectral synthesis. Figure 7 shows the synthesis of four Mn II lines in the NUV spectrum of BD+44°493.

To make a fair comparison with the Ito et al. (2013) abundances, we recomputed their optical abundances of Ti II, Mn II, and Ni I on the same $\log gf$ scale we used for the NUV lines. From the Wood et al. (2013) study, we find that the Ito et al. Ti II abundance would have decreased by only 0.01 dex. From lines in common with the Den Hartog et al. (2011) study, we find that the Ito et al. Mn II abundance would have increased by 0.08 dex.

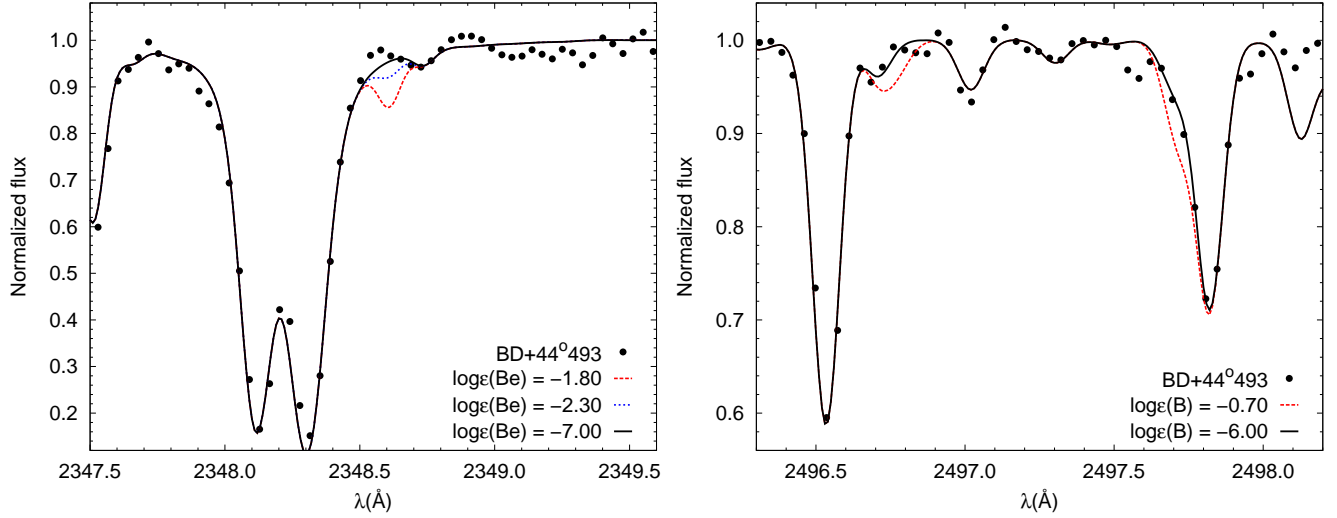


FIG. 5.— Left panel: The Be I line at 2348 Å, showing the 3- σ upper limit from this work ($\log \epsilon(\text{Be}) = -2.30$) and from Ito et al. (2013) ($\log \epsilon(\text{Be}) = -1.80$). Right panel: The B I line at 2497 Å, showing the 3- σ upper limit from this work ($\log \epsilon(\text{B}) = -0.70$). See text for discussion.

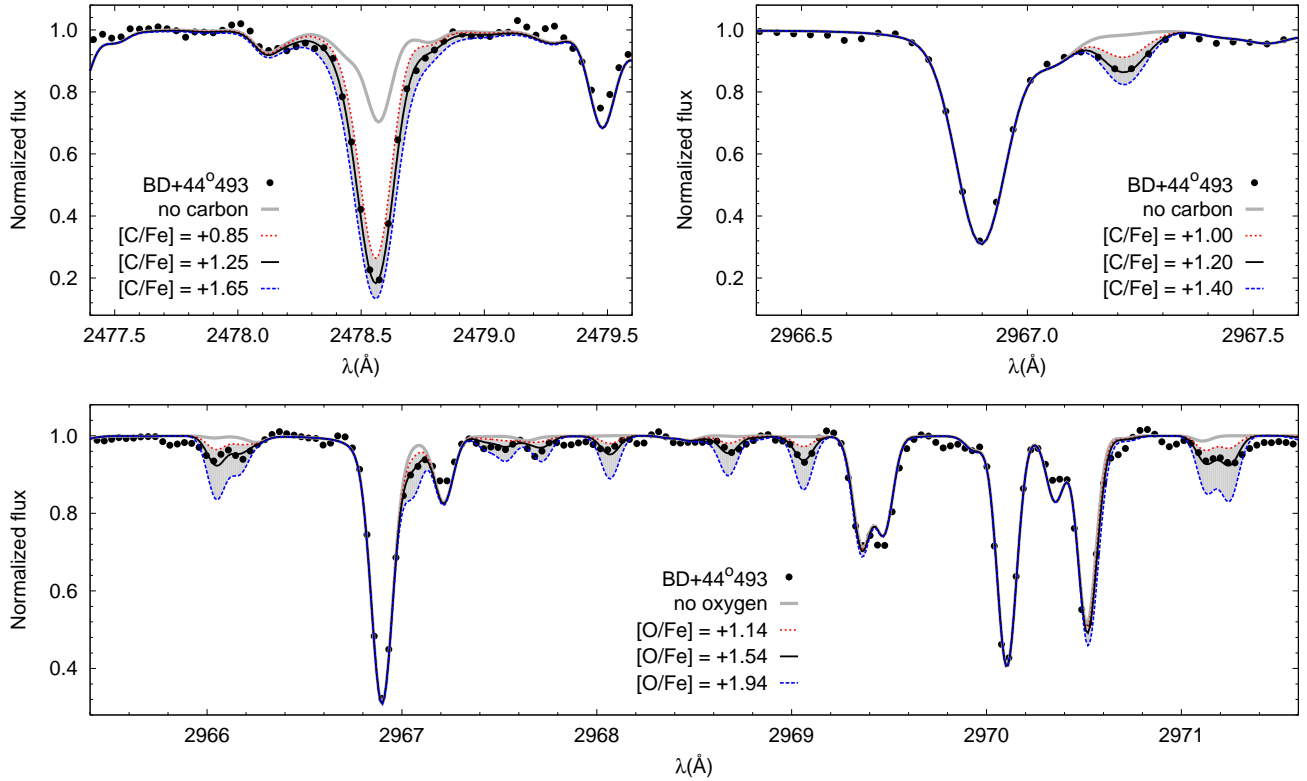


FIG. 6.— Upper left panel: Spectral synthesis of the atomic C I feature at 2478.5 Å. The dots represent the observed spectra, the solid line is the best abundance fit, and the dotted and dashed line are the lower and upper abundance limits, indicating the abundance uncertainty. The shaded area encompasses an 0.8 dex difference in [C/Fe]. The light gray line shows the Fe II line, located at essentially the same wavelength as the C I line. Upper right panel: C I feature at 2967.2 Å, with the shaded area representing a 0.4 dex difference in [C/Fe]. Lower panel: several OH features in the 2965-2972 Å range. The shaded area shows a 0.8 dex difference in [O/Fe].

From lines in common with the Wood et al. (2014) study, we find that the Ito et al. Ni I abundance would have had no change. There would also be no change for the Sc II abundance, since Ito et al. used the $\log g f$ values reported by Lawler & Dakin (1989).

As a result of this exercise, we find good agreement between the abundance ratios determined by this work and

those from Ito et al. (2013) – these are [Sc II/Fe] = +0.29, identical to that obtained from the optical work (+0.29); [Ti II/Fe] = +0.36 (+0.36 in the optical); [Cr II/Fe] = -0.09 (-0.22 in the optical); [Mn II/Fe] = -0.58 (-0.79 in the optical); and [Ni I/Fe] = -0.02 (+0.08 in the optical).

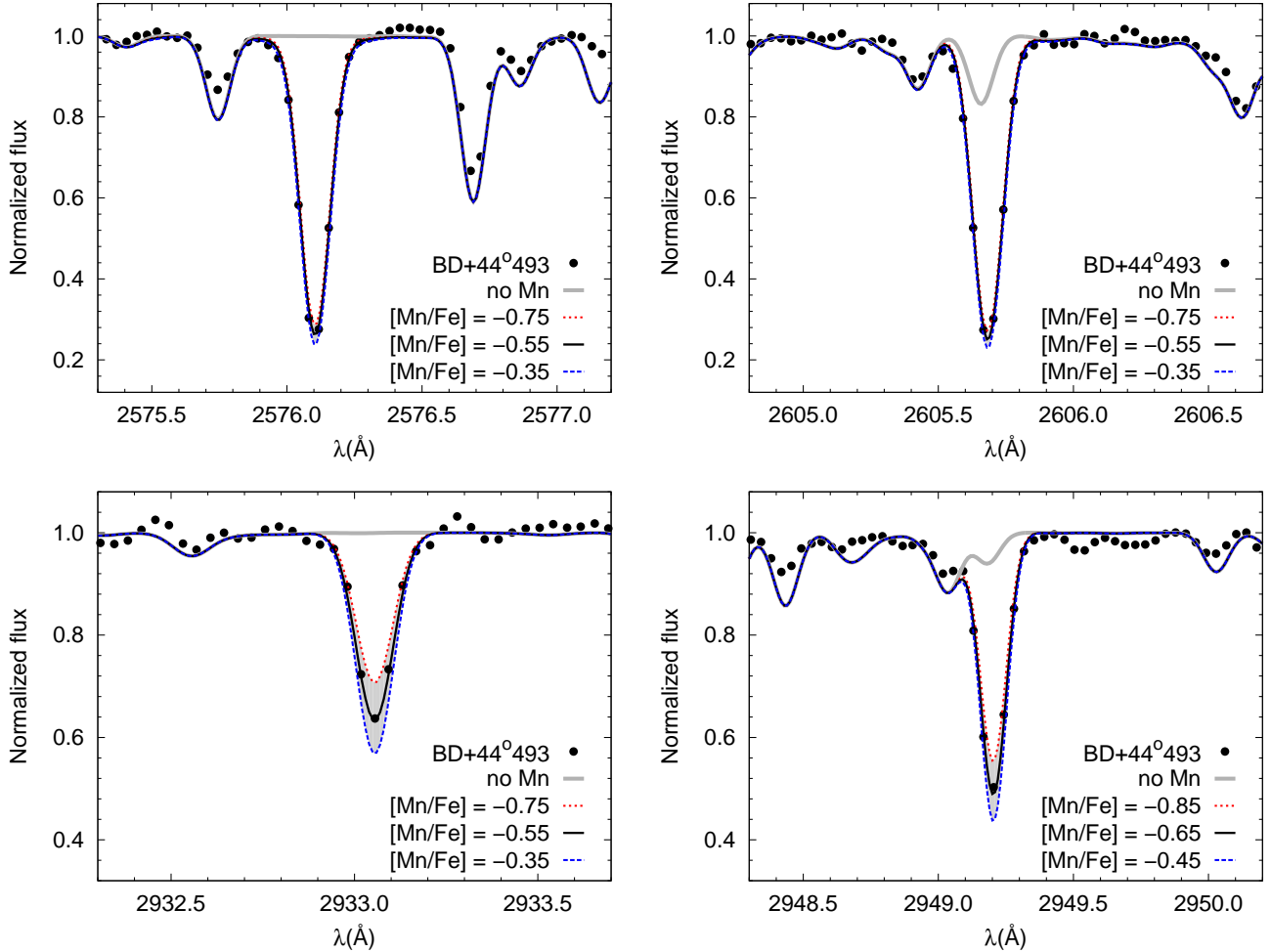


FIG. 7.— Spectral synthesis of four Mn II features. The dots represent the observed spectra, the solid line is the best abundance fit, and the dotted and dashed line are the lower and upper abundance limits, indicating the abundance uncertainty. The shaded area encompasses an 0.6 dex difference in $[\text{Mn}/\text{Fe}]$. The light gray line shows the synthesized spectrum in the absence of Mn.

3.4. The Neutron-Capture Elements

Only upper limits were determined in BD+44°493 for neutron-capture elements in the NUV region; Figure 8 shows examples of these limits for Zr II, Ge I, and Pt I. Figure 9 shows the comparison between the observed and the synthetic spectra around the Pb I 2833.05 Å feature. We determine a $3\text{-}\sigma$ ($2\text{-}\sigma$) upper limit of $\log \epsilon(\text{Pb}) < -0.23$ (< -0.42) from this line, assuming the poorly fit absorption features at 2832.9 Å and 2833.2 Å are noise, and not absorption lines. Our value confirms and strengthens the Ito et al. (2013) upper limit of $\log \epsilon(\text{Pb}) < -0.10$, estimated from the weak optical Pb I line at 4057.80 Å. Syntheses of both the $3\text{-}\sigma$ and $2\text{-}\sigma$ upper limits are shown in Figure 9, as well as for $\log \epsilon(\text{Pb}) = 0.00$ and $\log \epsilon(\text{Pb}) = -2.00$, for reference.

Figure 9 reveals that our upper limit on the abundance of Pb might indeed be too conservative, depending on the nature of the nearby noise features. The wavelength of the Pb I line is known to better than 1 mÅ (Wood & Andrew 1968), so these supposed noise features are not due to Pb I absorption. The feature at 2832.9 Å, however, is also observed in our spectra of HD 108317 and HD 196944 (see Figure 2), but the NIST database does not include any probable lines at this wavelength. The

known Fe II line at 2833.09 Å (Roederer et al. 2012a) does not appear in our spectrum of BD+44°493. The feature at 2833.2 Å may also appear in HD 108317 and HD 196944, but there it is weak. From examination of the summed spectra from the first four observations and the second four observations of BD+44°493 independently, these unidentified features appear in both. This indicates that they are not random noise spikes. If we do not treat these unfit features as noise, the upper limit on Pb becomes tighter – by at least several tenths of a dex – but it is still limited by our ability to correctly identify the continuum or other contaminants.

4. DISCUSSION AND CONCLUSIONS

Ito et al. (2013) have discussed in detail the importance of the low upper limit they derived for Be in the optical spectrum of BD+44°493, which we have now lowered by about a factor of three, to $\log \epsilon(\text{Be}) < -2.3$, based on our NUV *HST*/STIS measurements. Our estimate of the upper limit on B ($\log \epsilon(\text{B}) < -0.7$), is also of significance, since these limits are at the lowest level yet determined for very and extremely metal-poor stars. Figure 10 shows a comparison between Be and B abundances, as a function of $[\text{Fe}/\text{H}]$, for the upper limits determined in this work and data from Primas et al. (1999), Boesgaard et al.

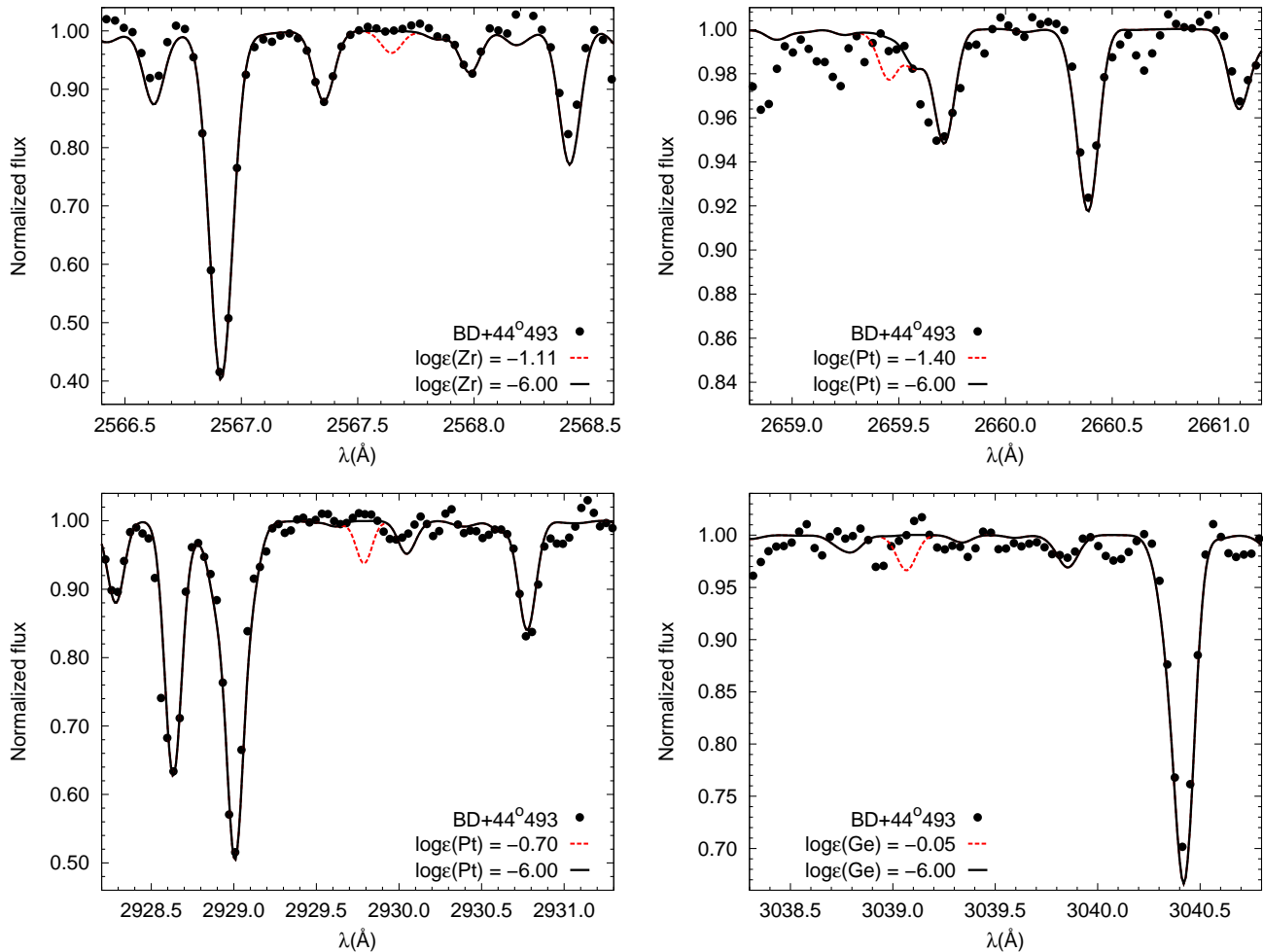


FIG. 8.— Examples of the $3\text{-}\sigma$ upper limits determined for Zr II, Pt I, and Ge I. The solid line shows the synthesized spectrum in the absence of the labeled features.

(2011), and the SAGA database (Suda et al. 2008). Individual references are listed in the caption of Figure 10.

How can we account for the low upper limits for Be and B, taken together with the fact that the Li abundance for BD+44°493 ($\log \epsilon(\text{Li}) = 1.0$, reported by Ito et al. 2013) is significantly below the level of the Spite Plateau? The low abundance of Li in this star, compared to the Spite Plateau value, could be a result of convective mixing with internal layers in which Li is fully depleted. Be might also be affected by mixing with material from layers that reach its burning temperature (3.0×10^6 K), which is slightly higher than that of Li (2.5×10^6 K). Compared to these two elements, B has an even higher burning temperature (5.0×10^6), and would be expected to be less affected by mixing, although such an interpretation depends on detailed modeling of stellar evolution during the subgiant phase. Alternatively, the very low upper limits of Be and B are consistent with the view that CEMP-no stars such as BD+44°493 may have formed in the very early universe, *prior* to the establishment of the level of cosmic-ray flux necessary to produce Be and B by spallation (for a more detailed discussion, see the review by Prantzos 2012). The low abundance of Li could then be accounted for by mixing of Li-astrated material (due to burning by first-generation stars) with primordial Li created by Big Bang nucleosynthesis (Piau et al. 2006).

This alternative receives some support from the recent observations of Li abundances below the Spite Plateau for CEMP-no stars by Hansen et al. (2014), including two stars with $T_{\text{eff}} = 6100$ K, presumably too warm for conventional Li-depletion from convective mixing to have taken place. It is worth recalling that Masseron et al. (2012) reports that the CEMP-no class *only* contains Li-depleted stars. Unfortunately, Be and B abundance estimates are not yet available for the CEMP-no stars of Hansen et al. (2014). Improved models and, in particular, additional observations of Be and B for CEMP-no stars, are necessary in order to constrain these ideas further. It should be noted that, as already discussed by Ito et al. (2013), the progenitor of BD+44°493 is unlikely to be a significant source of high-energy CNO nuclei that could yield lighter elements by spallation processes. This fact might be a useful constraint on the nature of the progenitor, most likely a faint (mixing and fallback) supernova, that produces the high C and O abundances found in BD+44°493.

We have discussed above that our measurement of $[\text{C}/\text{Fe}]$, based on the NUV atomic C I lines at 2478.56 Å and 2967.21 Å, provides an important validation of $[\text{C}/\text{Fe}]$ estimates for CEMP stars based on the CH G -band in the optical, as well as from C I lines in the NIR.

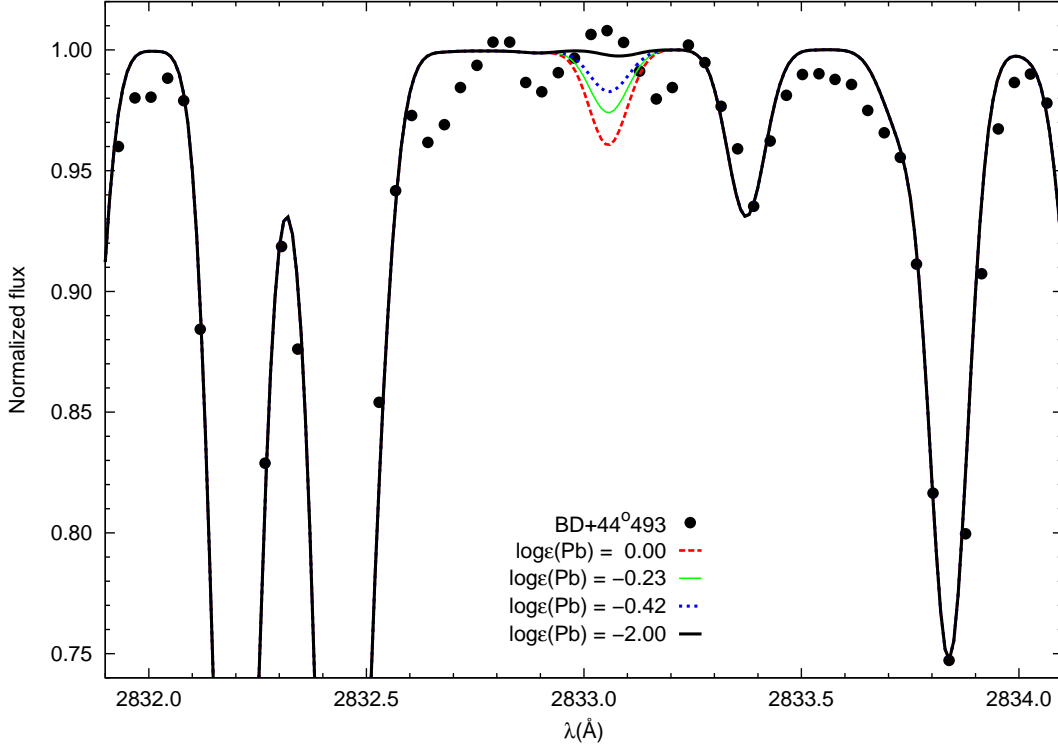


FIG. 9.— The Pb I line at 2833 Å, showing the $3\text{-}\sigma$ ($\log \epsilon(\text{Pb}) = -0.23$) and $2\text{-}\sigma$ ($\log \epsilon(\text{Pb}) = -0.42$) upper limits. See text for discussion.

Since this is the first determination of $[\text{C}/\text{Fe}]$ from NUV spectroscopy, it would clearly be important to carry out similar observations of additional bright CEMP stars, in order to test if this level of agreement holds for stars that are cooler, or more metal-rich, than BD+44°493.

The $[\text{Ni}/\text{Fe}]$ abundance ratio for BD+44°493 can also place further constraints on Galactic chemical-evolution models. By comparing this quantity with the value measured for the main-sequence turnoff star HD 84937 ($T_{\text{eff}} = 6300$ K, $\log g = 4.0$, $v_{\text{micro}} = 1.5$ km s $^{-1}$, and $[\text{Fe}/\text{H}] = -2.32$; Wood et al. 2014), one can see that, even though their metallicities are more than 1.5 dex apart, their $[\text{Ni}/\text{Fe}]$ ratios exhibit only a 0.05 dex difference. This corroborates the predicted plateau for Ni abundances as a function of the metallicity from the theoretical models of Kobayashi et al. (2011a), and can set observational limits on the Galactic initial mass function and yields from both core-collapse supernovae and hypernovae.

Figure 11 shows a comparison between a set of s - and r -process templates and the upper limits on neutron-capture elements determined in this work. Also shown are the optical abundances from Ito et al. (2013). These are used to normalize the models (to Sr in the upper panel and to Ba in the lower panel). The template for the weak component of the r -process is the metal-poor giant HD 122563 (Honda et al. 2006; Roederer et al. 2012b). The template for the main component of the r -process is the metal-poor giant CS 22892-052 (Snedden et al. 2003, 2009; Cowan et al. 2005; Roederer et al. 2009). The template for the s -process shows the AGB yields from the model presented in Placco et al. (2013), with $M = 1.3 M_{\odot}$ and $[\text{Fe}/\text{H}] = -2.5$ ¹⁵. This is necessary due to the fact that, in contrast to the “universal” r -process, the s -process abundances are highly dependent on metallicity. These templates are not intended as firm representations of the expected nucleosynthesis outcomes, since, for ex-

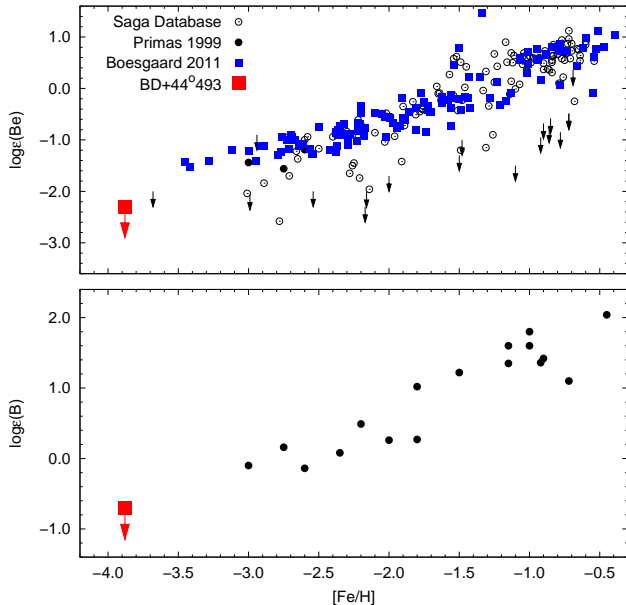


FIG. 10.— Be and B abundances (and upper limits), as a function of the metallicity, for BD+44°493 and the stars listed in Primas et al. (1999), Boesgaard et al. (2011), and the SAGA database (Suda et al. 2008). Individual references include: Tan et al. (2009), Boesgaard & Novicki (2005), Boesgaard & Novicki (2006), Boesgaard (2007), García Pérez & Primas (2006), Rich & Boesgaard (2009), and Smiljanic et al. (2009).

¹⁵ Intermediate-mass AGB yields are beyond the scope of the current work, and were not added to this analysis.

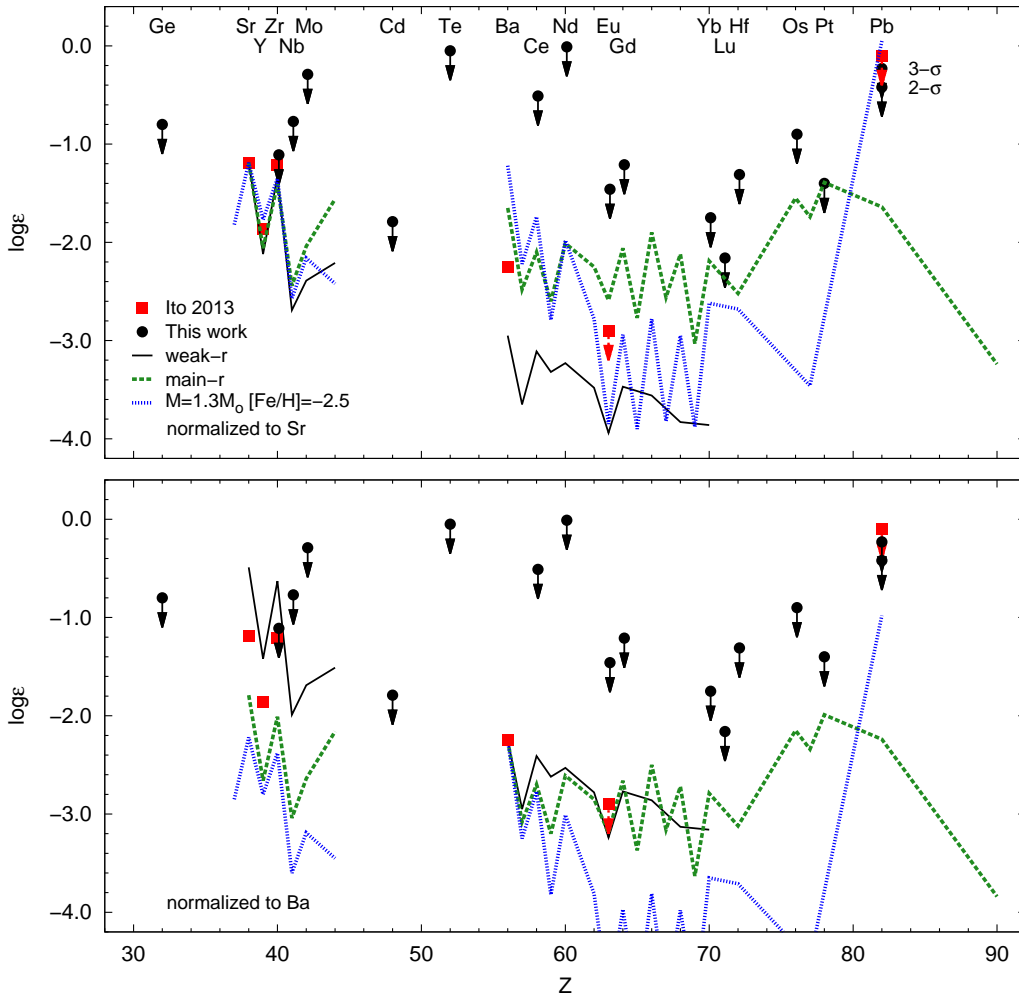


FIG. 11.— Comparison between upper limits determined from this work, abundances from Ito et al. (2013), and stellar templates for the solar r -process and the $1.3 M_{\odot}$, $[\text{Fe}/\text{H}] = -2.5$ AGB yields described in Placco et al. (2013). Upper panel: Models normalized to the Sr optical abundance. Lower panel: Models normalized to the Ba optical abundance.

ample, the yields depend on the physical conditions at the time the nucleosynthesis events took place.

Stars with metallicities as low as BD+44°493 do not exhibit enhancements of s -process material (e.g., Simmerer et al. 2004), at least none have been identified to date. At somewhat higher metallicities, the s -process elements in CEMP- s stars typically show substantial enhancements relative to the solar abundance ratios (e.g., Aoki et al. 2002), which are attributed to a mass-transfer event from a companion star that passed through the AGB phase of evolution. At lower metallicity, the high neutron-to-seed ratios are expected to drive the flow to the most massive stable elements that can be produced by the s -process, Pb and Bi (e.g., Gallino et al. 1998). Enhanced Pb abundances are considered unmistakable signatures of the operation of s -process nucleosynthesis in a low-metallicity environment.

To the best of our knowledge, Pb has not been detected for any stars with $[\text{Fe}/\text{H}] < -3.2$ (see, e.g., Figure 3 of Roederer et al. 2010a). Our results do not change this finding. Figure 12 shows the $[\text{Pb}/\text{Fe}]$, $[\text{Ba}/\text{Fe}]$, and $[\text{Pb}/\text{Ba}]$ values for BD+44°493, compared with four different model prescriptions from Bisterzo et al. (2010). Even though BD+44°493 exhibits a clear lack of Pb and

Ba when compared to the models, the upper limit we place on Pb, relative to barium, $[\text{Pb}/\text{Ba}] < +2.5$, is on the cusp of excluding s -process nucleosynthesis in low-mass low-metallicity AGB stars with the highest neutron exposures possible.

This is not yet definitive evidence against an s -process origin of the neutron-capture elements in BD+44°493; however, the lack of significant radial-velocity variations (Carney et al. 2003; Ito et al. 2013, spanning over 25 years) and the sub-solar $[\text{Sr}/\text{Fe}]$ and $[\text{Ba}/\text{Fe}]$ ratios are suggestive that enrichment from an unseen companion that passed through the AGB phase of evolution appears extremely unlikely, calling for non-AGB sources, such as spinstars or faint supernovae explosions that undergo mixing and fallback.

Some form of r -process nucleosynthesis may have been the dominant production mechanism for the neutron-capture elements observed in BD+44°493, and other stars at extremely low metallicity (e.g., Truran 1981). Barium is the heaviest element detected in BD+44°493. The abundance pattern presented in the bottom panel of Figure 11 cannot exclude that the neutron-capture abundance pattern in BD+44°493 resembles that found in the main or weak components of the r -process. Roed-

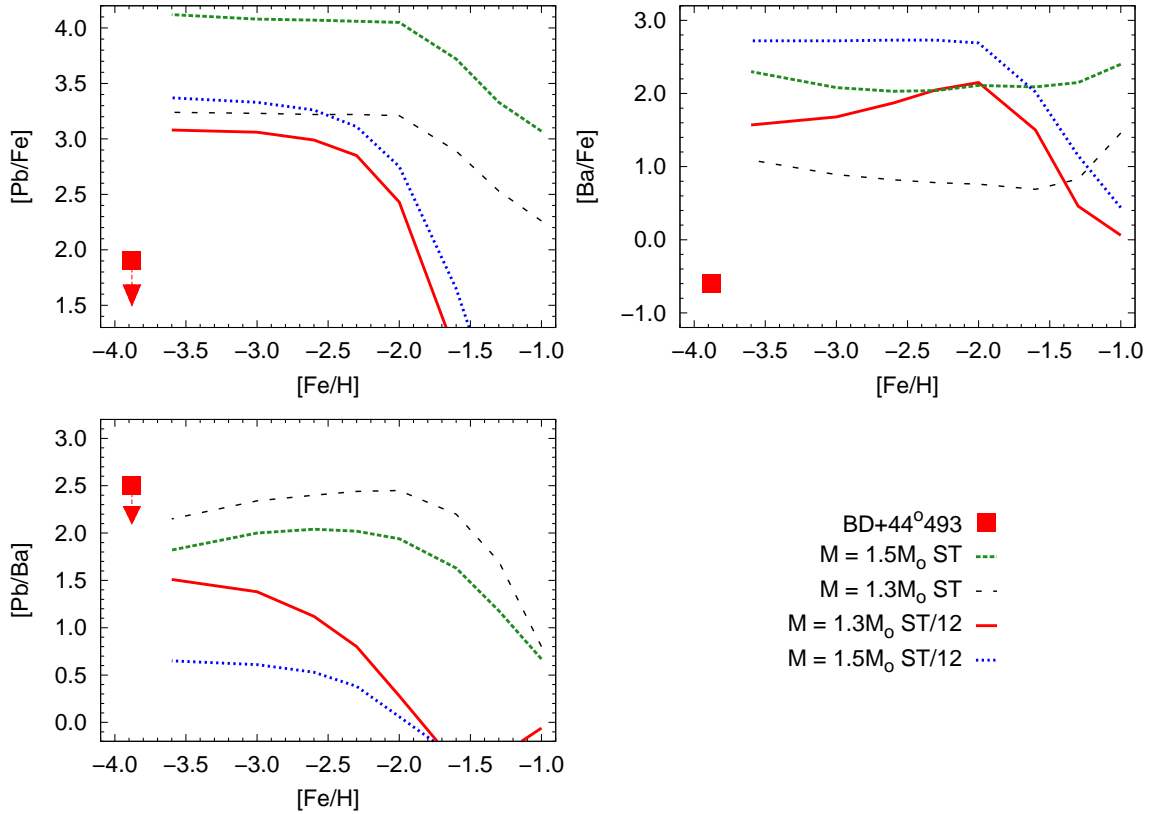


FIG. 12.— $[\text{Pb}/\text{Fe}]$ (this work), $[\text{Ba}/\text{Fe}]$, and $[\text{Pb}/\text{Ba}]$ (Ito et al. 2013) compared with AGB theoretical predictions for two different initial masses and ^{13}C -pocket efficiencies. Data were taken from Tables B5 and B6 of Bisterzo et al. (2010).

erer et al. (2014b) also reached this conclusion, based on their analysis of optical spectra of BD+44°493 and other members of the CEMP-no sub-class of stars.

BD+44°493 is also the most metal-poor star where the Ge abundance can be reasonably evaluated. The upper limit on the Ge abundance in BD+44°493 we obtain is only about a factor of three higher than the mean $[\text{Ge}/\text{Fe}]$ ratio found for stars with $-3.0 < [\text{Fe}/\text{H}] < -1.6$ (see Figure 3 of Roederer 2012). This indicates that Ge was not manufactured in large quantities by the stars that produced the metals in BD+44°493. The primary nucleosynthesis mechanism of Ge assumed for the stars with $-3.0 < [\text{Fe}/\text{H}] < -1.6$, some form of explosive or charged-particle nucleosynthesis, is not excluded as a possible source for whatever Ge may be present in BD+44°493.

The Te upper limit we obtain is still about 2 dex higher than what might be required to secure a Te detection in BD+44°493, based on the Ba abundance in BD+44°493 and the $\log \epsilon$ (Te/Ba) ratios reported by Roederer et al. (2012a). Similarly, the Cd upper limit is about 1 dex higher than what might be required to secure a Cd detection in BD+44°493. If the 3rd r -process peak elements in BD+44°493 are assumed to follow a scaled-solar r -process abundance pattern, the Pt upper limit is about 0.5 dex higher than what might be required to secure a Pt detection in BD+44°493. If the 3rd r -process peak elements in BD+44°493 are deficient relative to Ba and the rare-earth elements, as found in the metal-poor giants HD 122563 and HD 128279 by Roederer et al. (2012b), it would be even more challenging to secure a Pt detec-

tion in BD+44°493. Te and Pt are expected to be two of the most abundant elements heavier than Zr (Snedden et al. 2008), yet it is unlikely that either of these elements can be detected in BD+44°493. This highlights the challenge of firmly establishing the nucleosynthetic origins of the elements heavier than the iron group for extremely metal-poor CEMP-no stars.

V.M.P. acknowledges support from the Gemini Observatory. T.C.B. and H.S. acknowledge partial support for this work from PHY 08-22648; Physics Frontier Center/Joint Institute of Nuclear Astrophysics (JINA), awarded by the US National Science Foundation. A.F. is supported by NSF CAREER grant AST-1255160. W.A. was supported by the JSPS Grants-in-Aid for Scientific Research (23224004). Generous support for Program GO-12554 has been provided by NASA through a grant from the Space Telescope Science Institute, which is operated by the Association of Universities for Research in Astronomy, Inc., under NASA contract NAS 5-26555.

REFERENCES

- Allen, D. M., Ryan, S. G., Rossi, S., Beers, T. C., & Tsangarides, S. A. 2012, *A&A*, 548, A34
- Aoki, W., Ryan, S. G., Norris, J. E., et al. 2002, *ApJ*, 580, 1149
- Aoki, W., Beers, T. C., Christlieb, N., et al. 2007, *ApJ*, 655, 492
- Arlandini, C., Käppeler, F., Wisshak, K., et al. 1999, *ApJ*, 525, 886
- Asplund, M. 2005, *ARA&A*, 43, 481
- Asplund, M., Grevesse, N., Sauval, A. J., & Scott, P. 2009, *ARA&A*, 47, 481
- Barbuy, B., Cayrel, R., Spite, M., et al. 1997, *A&A*, 317, L63
- Beers, T. C., Preston, G. W., & Shectman, S. A. 1992, *AJ*, 103, 1987
- Beers, T. C., & Christlieb, N. 2005, *ARA&A*, 43, 531
- Bergeson, S. D., & Lawler, J. E. 1993, *ApJ*, 408, 382
- Biémont, E., Palmeri, P., & Quinet, P. 1999, *Ap&SS*, 269, 635
- Biémont, E., Garnir, H. P., Palmeri, P., Li, Z. S., & Svanberg, S. 2000, *MNRAS*, 312, 116
- Bisterzo, S., Gallino, R., Straniero, O., Cristallo, S., & Käppeler, F. 2010, *MNRAS*, 404, 1529
- . 2012, *MNRAS*, 422, 849
- Boesgaard, A. M., & Novicki, M. C. 2005, *ApJ*, 633, L125
- . 2006, *ApJ*, 641, 1122
- Boesgaard, A. M. 2007, *ApJ*, 667, 1196
- Boesgaard, A. M., Rich, J. A., Levesque, E. M., & Bowler, B. P. 2011, *ApJ*, 743, 140
- Busso, M., Gallino, R., & Wasserburg, G. J. 1999, *ARA&A*, 37, 239
- Caffau, E., Bonifacio, P., François, P., et al. 2011, *A&A*, 534, A4
- Carney, B. W., Latham, D. W., Stefanik, R. P., Laird, J. B., & Morse, J. A. 2003, *AJ*, 125, 293
- Carollo, D., Beers, T. C., Bovy, J., et al. 2012, *ApJ*, 744, 195
- Castelli, F., & Kurucz, R. L. 2004, *ArXiv Astrophysics e-prints*, arXiv:astro-ph/0405087
- Chiappini, C. 2013, *Astronomische Nachrichten*, 334, 595
- Christlieb, N., Bessell, M. S., Beers, T. C., et al. 2002, *Nature*, 419, 904
- Cohen, J. G., Shectman, S., Thompson, I., et al. 2005, *ApJ*, 633, L109
- Cohen, J. G., McWilliam, A., Shectman, S., et al. 2006, *AJ*, 132, 137
- Cohen, J. G., Christlieb, N., Thompson, I., et al. 2013, *ApJ*, 778, 56
- Collet, R., Asplund, M., & Trampedach, R. 2007, *A&A*, 469, 687
- Cooke, R., Pettini, M., Steidel, C. C., Rudie, G. C., & Nissen, P. E. 2011, *MNRAS*, 417, 1534
- Cowan, J. J., Sneden, C., Beers, T. C., et al. 2005, *ApJ*, 627, 238
- Den Hartog, E. A., Herd, M. T., Lawler, J. E., et al. 2005, *ApJ*, 619, 639
- Den Hartog, E. A., Lawler, J. E., Sneden, C., & Cowan, J. J. 2006, *ApJS*, 167, 292
- Den Hartog, E. A., Lawler, J. E., Sobek, J. S., Sneden, C., & Cowan, J. J. 2011, *ApJS*, 194, 35
- Fedchak, J. A., & Lawler, J. E. 1999, *ApJ*, 523, 734
- Frebel, A., Aoki, W., Christlieb, N., et al. 2005, *Nature*, 434, 871
- Frebel, A., Christlieb, N., Norris, J. E., Aoki, W., & Asplund, M. 2006a, *ApJ*, 638, L17
- Frebel, A., Christlieb, N., Norris, J. E., et al. 2006b, *ApJ*, 652, 1585
- Frebel, A., Johnson, J. L., & Bromm, V. 2007, *MNRAS*, 380, L40
- Frebel, A., & Norris, J. E. 2013, *Planets, Stars and Stellar Systems*. Volume 5: Galactic Structure and Stellar Populations, 55
- Fuhr, J. R., & Wiese, W. L. 2009, published in the *CRC Handbook of Chemistry and Physics*
- Gallino, R., Arlandini, C., Busso, M., et al. 1998, *ApJ*, 497, 388
- García Pérez, A. E., & Primas, F. 2006, *A&A*, 447, 299
- Hansen, T., Andersen, J., & Nordström, B. 2013, in *Proceedings of Science (NIC XII)*, Vol. 193
- Hansen, T., Hansen, C. J., Christlieb, N., et al. 2014, *ApJ*, 787, 162
- Herwig, F. 2005, *ARA&A*, 43, 435
- Hill, V., Barbuy, B., Spite, M., et al. 2000, *A&A*, 353, 557
- Hirschi, R. 2007, *A&A*, 461, 571
- Honda, S., Aoki, W., Ishimaru, Y., Wanajo, S., & Ryan, S. G. 2006, *ApJ*, 643, 1180
- Ito, H., Aoki, W., Beers, T. C., et al. 2013, *ApJ*, 773, 33
- Jonsell, K., Barklem, P. S., Gustafsson, B., et al. 2006, *A&A*, 451, 651
- Jorissen, A., Van Eck, S., Mayor, M., & Udry, S. 1998, *A&A*, 332, 877
- Keller, S. C., Bessell, M. S., Frebel, A., et al. 2014, *Nature*, 506, 463
- Kennedy, C. R., Sivarani, T., Beers, T. C., et al. 2011, *AJ*, 141, 102
- Kimble, R. A., Woodgate, B. E., Bowers, C. W., et al. 1998, *ApJ*, 492, L83
- Kiselman, D., & Carlsson, M. 1996, *A&A*, 311, 680
- Kobayashi, C., Karakas, A. I., & Umeda, H. 2011a, *MNRAS*, 414, 3231
- Kobayashi, C., Tominaga, N., & Nomoto, K. 2011b, *ApJ*, 730, L14
- Kramida, A., Yu. Ralchenko, Reader, J., & and NIST ASD Team. 2013, *NIST Atomic Spectra Database (ver. 5.1)*, [Online]. Available: <http://physics.nist.gov/asd> [2014, April 7]. National Institute of Standards and Technology, Gaithersburg, MD.
- Kupka, F., Piskunov, N., Ryabchikova, T. A., Stempels, H. C., & Weiss, W. W. 1999, *A&AS*, 138, 119
- Kurucz, R. 1993, *Diatomic Molecular Data for Opacity Calculations*. Kurucz CD-ROM No. 15. Cambridge, Mass.: Smithsonian Astrophysical Observatory, 1993., 15
- Kurucz, R., & Bell, B. 1995, *Atomic Line Data (R.L. Kurucz and B. Bell) Kurucz CD-ROM No. 23*. Cambridge, Mass.: Smithsonian Astrophysical Observatory, 1995., 23
- Lawler, J. E., & Dakin, J. T. 1989, *Journal of the Optical Society of America B Optical Physics*, 6, 1457
- Lawler, J. E., den Hartog, E. A., Labby, Z. E., et al. 2007, *ApJS*, 169, 120
- Lawler, J. E., Guzman, A., Wood, M. P., Sneden, C., & Cowan, J. J. 2013, *ApJS*, 205, 11
- Lee, Y. S., Beers, T. C., Masseron, T., et al. 2013, *AJ*, 146, 132
- Ljung, G., Nilsson, H., Asplund, M., & Johansson, S. 2006, *A&A*, 456, 1181
- Lucatello, S., Tsangarides, S., Beers, T. C., et al. 2005, *ApJ*, 625, 825
- Lucatello, S., Beers, T. C., Christlieb, N., et al. 2006, *ApJ*, 652, L37
- Lugaro, M., Karakas, A. I., Stancliffe, R. J., & Rijs, C. 2012, *ApJ*, 747, 2
- Malcheva, G., Blagoev, K., Mayo, R., et al. 2006, *MNRAS*, 367, 754
- Marsteller, B., Beers, T. C., Rossi, S., et al. 2005, *Nuclear Physics A*, 758, 312
- Masseron, T., van Eck, S., Famaey, B., et al. 2006, *A&A*, 455, 1059
- Masseron, T., Johnson, J. A., Plez, B., et al. 2010, *A&A*, 509, A93
- Masseron, T., Johnson, J. A., Lucatello, S., et al. 2012, *ApJ*, 751, 14
- McClure, R. D. 1983, *ApJ*, 268, 264
- McClure, R. D., & Woodsworth, A. W. 1990, *ApJ*, 352, 709
- Meynet, G., Ekström, S., & Maeder, A. 2006, *A&A*, 447, 623
- Meynet, G., Hirschi, R., Ekstrom, S., et al. 2010, *A&A*, 521, A30
- Morton, D. C. 2000, *ApJS*, 130, 403
- Nilsson, H., & Ivarsson, S. 2008, *A&A*, 492, 609
- Norris, J. E., Ryan, S. G., & Beers, T. C. 1997, *ApJ*, 488, 350
- Norris, J. E., Christlieb, N., Korn, A. J., et al. 2007, *ApJ*, 670, 774
- Norris, J. E., Bessell, M. S., Yong, D., et al. 2013, *ApJ*, 762, 25
- Piau, L., Beers, T. C., Balsara, D. S., et al. 2006, *ApJ*, 653, 300
- Placco, V. M., Kennedy, C. R., Beers, T. C., et al. 2011, *AJ*, 142, 188
- Placco, V. M., Frebel, A., Beers, T. C., et al. 2013, *ApJ*, 770, 104
- . 2014, *ApJ*, 781, 40
- Prantzos, N. 2012, *A&A*, 542, A67
- Primas, F., Duncan, D. K., Peterson, R. C., & Thorburn, J. A. 1999, *A&A*, 343, 545
- Quinet, P., Palmeri, P., Biémont, É., et al. 2006, *A&A*, 448, 1207
- Rich, J. A., & Boesgaard, A. M. 2009, *ApJ*, 701, 1519
- Roederer, I. U., Lawler, J. E., Sneden, C., et al. 2008, *ApJ*, 675, 723
- Roederer, I. U., Kratz, K., Frebel, A., et al. 2009, *ApJ*, 698, 1963

- Roederer, I. U., Cowan, J. J., Karakas, A. I., et al. 2010a, *ApJ*, 724, 975
- Roederer, I. U., Sneden, C., Lawler, J. E., & Cowan, J. J. 2010b, *ApJ*, 714, L123
- Roederer, I. U. 2012, *ApJ*, 756, 36
- Roederer, I. U., Lawler, J. E., Cowan, J. J., et al. 2012a, *ApJ*, 747, L8
- Roederer, I. U., Lawler, J. E., Sobeck, J. S., et al. 2012b, *ApJS*, 203, 27
- Roederer, I. U., Preston, G. W., Thompson, I. B., Shectman, S. A., & Sneden, C. 2014a, *ApJ*, 784, 158
- Roederer, I. U., Preston, G. W., Thompson, I. B., et al. 2014b, *AJ*, 147, 136
- Rossi, S., Beers, T. C., & Sneden, C. 1999, in *Astronomical Society of the Pacific Conference Series*, Vol. 165, *The Third Stromlo Symposium: The Galactic Halo*, ed. B. K. Gibson, R. S. Axelrod, & M. E. Putman, 264
- Rossi, S., Beers, T. C., Sneden, C., et al. 2005, *AJ*, 130, 2804
- Schuler, S. C., Margheim, S. J., Sivarani, T., et al. 2008, *AJ*, 136, 2244
- Sikström, C. M., Pihlemark, H., Nilsson, H., et al. 2001, *Journal of Physics B Atomic Molecular Physics*, 34, 477
- Simmerer, J., Sneden, C., Cowan, J. J., et al. 2004, *ApJ*, 617, 1091
- Smiljanic, R., Pasquini, L., Bonifacio, P., et al. 2009, *A&A*, 499, 103
- Sneden, C. A. 1973, PhD thesis, The University of Texas at Austin.
- Sneden, C., Cowan, J. J., Burris, D. L., & Truran, J. W. 1998, *ApJ*, 496, 235
- Sneden, C., Cowan, J. J., Lawler, J. E., et al. 2003, *ApJ*, 591, 936
- Sneden, C., Cowan, J. J., & Gallino, R. 2008, *ARA&A*, 46, 241
- Sneden, C., Lawler, J. E., Cowan, J. J., Ivans, I. I., & Den Hartog, E. A. 2009, *ApJS*, 182, 80
- Sobeck, J. S., Kraft, R. P., Sneden, C., et al. 2011, *AJ*, 141, 175
- Spite, M., Caffau, E., Bonifacio, P., et al. 2013, *A&A*, 552, A107
- Stancliffe, R. J., & Glebbeek, E. 2008, *MNRAS*, 389, 1828
- Starkenburg, E., Shetrone, M. D., McConnachie, A. W., & et al. 2014, *MNRAS*, 441, 1217
- Suda, T., Katsuta, Y., Yamada, S., et al. 2008, *PASJ*, 60, 1159
- Takeda, Y., & Takada-Hidai, M. 2013, *PASJ*, 65, 65
- Tan, K. F., Shi, J. R., & Zhao, G. 2009, *MNRAS*, 392, 205
- Tominaga, N., Umeda, H., & Nomoto, K. 2007, *ApJ*, 660, 516
- Truran, J. W. 1981, *A&A*, 97, 391
- Umeda, H., & Nomoto, K. 2005, *ApJ*, 619, 427
- Waters, C. Z., & Hollek, J. K. 2013, *PASP*, 125, 1164
- Wood, D. R., & Andrew, K. L. 1968, *Journal of the Optical Society of America (1917-1983)*, 58, 818
- Wood, M. P., Lawler, J. E., Sneden, C., & Cowan, J. J. 2013, *ApJS*, 208, 27
- . 2014, *ApJS*, 211, 20
- Woodgate, B. E., Kimble, R. A., Bowers, C. W., et al. 1998, *PASP*, 110, 1183
- Yanny, B., Rockosi, C., Newberg, H. J., et al. 2009, *AJ*, 137, 4377
- York, D. G., Adelman, J., Anderson, Jr., J. E., et al. 2000, *AJ*, 120, 1579

TABLE 1
EQUIVALENT WIDTH MEASUREMENTS

λ (Å)	χ (eV)	$\log gf$	W (mÅ)	$\log \epsilon_W$	$\log \epsilon_{syn}$
Fe I					
2283.30	0.12	-2.22	21.10	3.62	3.70
2283.66	0.11	-2.22	3.70
2293.85	0.09	-2.37	13.10	3.43	3.60
2294.41	0.11	-1.54	43.40	3.71	3.65
2296.93	0.11	-2.02	29.60	3.68	3.70
2297.79	0.05	-1.10	52.80	3.59	3.60
2298.66	0.11	-2.42	13.90	3.54	3.60
2299.22	0.09	-1.55	38.00	3.48	3.65
2320.36	0.05	-0.99	57.80	3.66	3.65
2350.41	0.00	-3.03	7.30	3.67	...
2369.46	0.11	-2.19	19.10	3.49	3.50
2371.43	0.09	-1.95	33.30	3.67	3.70
2374.52	0.12	-2.10	22.90	3.53	3.60
2389.97	0.09	-1.57	39.70	3.50	3.60
2443.87	0.86	-1.24	28.00	3.58	3.65
2445.21	0.86	-2.02	5.40	3.40	...
2453.48	0.92	-0.92	27.90	3.31	...
2457.60	0.86	-0.32	48.00	3.32	...
2462.18	0.05	-1.30	49.80	3.54	3.60
2462.65	0.00	-0.32	78.40	3.46	3.60
2463.73	0.96	-1.13	20.60	3.33	...
2468.88	0.86	-0.62	42.50	3.41	3.55
2470.97	0.92	-1.62	8.40	3.27	...
2472.89	0.05	-0.08	99.50	3.65	3.60
2485.99	0.92	-1.61	10.30	3.36	3.60
2486.69	0.96	-0.91	28.50	3.35	3.50
2487.07	1.01	-0.75	32.90	3.38	3.55
2487.37	0.09	-1.90	31.60	3.51	3.55
2491.16	0.11	+0.13	104.30	3.55	3.60
2495.87	0.86	-1.76	12.70	3.56	3.65
2496.53	0.92	-0.66	39.10	3.37	3.50
2501.13	0.00	-0.35	81.70	3.55	3.60
2501.69	0.86	-1.51	23.50	3.69	3.70
2507.90	0.96	-0.79	34.50	3.40	3.50
2508.75	0.99	-1.95	3.65
2517.66	0.99	-0.98	32.80	3.57	3.65
2518.10	0.09	-0.26	75.10	3.37	3.60
2519.63	1.01	-1.20	19.70	3.41	3.65
2522.48	0.92	-1.92	12.20	3.76	3.70
2522.85	0.00	+0.26	3.70
2530.69	0.09	-2.37	3.70
2543.92	2.45	+0.70	31.40	3.32	3.55
2552.61	0.11	-2.52	15.30	3.62	3.65
2556.86	0.86	-2.02	3.55
2560.56	1.01	-2.11	3.65
2569.74	0.99	-2.24	3.10	3.47	...
2576.69	0.86	-0.91	35.90	3.43	3.55
2584.54	0.86	-0.39	51.00	3.42	3.60
2610.75	0.09	-2.96	5.10	3.45	3.70
2612.77	0.05	-2.59	17.30	3.68	3.70
2618.02	0.96	-0.97	38.60	3.66	3.65
2618.71	0.00	-2.43	14.20	3.35	3.50
2623.37	0.11	-2.57	3.65
2623.53	0.96	-0.70	48.40	3.72	3.60
2632.24	0.99	-1.20	25.60	3.54	3.60
2632.59	0.09	-2.33	23.80	3.67	3.65
2635.81	0.99	-0.81	43.60	3.69	3.60
2636.48	0.92	-2.04	6.00	3.49	3.55
2641.03	2.45	-1.25	1.70	3.72	...
2644.00	1.01	-0.91	29.50	3.38	3.50
2647.56	0.05	-2.42	18.50	3.55	3.60
2651.71	0.96	-2.04	5.80	3.51	3.70
2656.14	2.40	-0.59	3.70	3.36	3.60
2656.79	1.49	-1.77	3.90	3.61	3.65
2660.40	0.99	-2.33	5.40	3.80	3.70
2662.06	0.96	-1.61	9.00	3.30	...
2679.06	0.86	-0.75	50.90	3.72	3.60
2680.45	0.99	-1.74	7.40	3.35	3.50
2689.21	0.92	-0.89	41.70	3.61	3.60
2690.07	0.00	-2.72	11.00	3.48	3.55
2699.11	0.92	-1.26	24.50	3.47	3.60
2710.54	1.61	-1.33	4.30	3.34	3.60
2714.87	0.96	-2.19	3.50	3.41	3.60

TABLE 1 — *Continued*

λ (Å)	χ (eV)	$\log gf$	W (mÅ)	$\log \epsilon_W$	$\log \epsilon_{syn}$
2723.58	0.09	-0.72	73.50	3.66	3.70
2726.05	1.01	-1.21	19.60	3.37	3.55
2728.02	0.92	-1.46	19.10	3.50	3.55
2735.47	0.92	-0.40	54.50	3.53	...
2737.31	0.11	-0.61	3.70
2744.07	0.12	-0.98	3.65
2754.03	0.99	-1.38	3.60
2755.18	2.43	-1.28	3.65
2756.27	0.05	-2.17	3.65
2756.33	0.11	-1.09	3.65
2759.81	1.01	-1.58	12.00	3.45	3.55
2772.07	0.86	-1.53	3.65
2772.11	0.09	-1.48	3.65
2813.29	0.92	-0.35	3.60
2823.28	0.96	-0.90	3.60
2827.89	0.05	-2.80	8.00	3.43	3.60
2838.12	0.99	-1.11	3.55
2936.90	0.00	-0.79	3.50
2959.99	2.69	-0.07	9.90	3.55	3.55
2965.25	0.12	-1.34	3.70
2970.10	0.11	-1.15	3.65
2970.12	0.09	-1.87	3.65
2983.57	0.00	-0.58	3.65
2994.43	0.05	-0.53	3.70
2994.50	0.12	-2.22	3.70
2999.51	0.86	-0.60	3.70
3000.45	1.49	-1.09	3.50
3008.14	0.11	-0.84	3.60
3016.18	0.99	-1.44	3.60
3021.07	0.05	-0.36	3.60
3026.46	0.99	-1.12	3.60
3037.39	0.11	-0.70	3.60
3042.66	0.99	-1.30	3.60
3047.61	0.09	-0.56	79.70	3.45	3.60
3059.09	0.05	-0.69	3.70
Fe II					
2331.31	0.23	-0.68	110.40	3.58	3.70
2354.89	0.35	-1.05	84.70	3.49	3.65
2359.11	0.11	-0.60	3.70
2359.60	2.68	-0.73	21.40	3.57	3.55
2360.00	0.23	-0.52	3.70
2360.29	0.30	-0.51	3.70
2361.73	2.69	-0.79	12.30	3.31	3.50
2368.60	0.35	-0.69	102.70	3.58	3.55
2370.50	0.39	-1.23	76.10	3.68	3.70
2384.39	0.39	-0.96	85.30	3.60	3.70
2399.24	0.08	-0.14	3.65
2422.69	3.89	+0.01	7.80	3.45	3.60
2429.39	2.70	-0.61	26.70	3.63	3.60
2430.08	2.83	+0.23	40.50	3.37	...
2432.87	4.08	+0.55	12.90	3.36	3.55
2433.50	2.68	-0.86	23.80	3.76	3.70
2446.47	2.66	-0.42	31.30	3.54	3.60
2447.20	3.89	-0.21	8.50	3.71	3.65
2463.28	3.15	-0.19	23.20	3.54	3.60
2464.91	3.23	-0.09	22.00	3.48	3.60
2468.30	2.68	-1.05	15.90	3.67	3.70
2470.41	3.23	-0.48	11.20	3.47	3.50
2470.67	2.83	-0.07	40.50	3.65	3.60
2476.27	2.69	-1.05	12.70	3.56	3.60
2497.82	3.23	-0.03	23.10	3.44	3.60
2502.39	3.22	+0.03	23.80	3.40	3.55
2506.09	3.20	-0.03	20.10	3.32	3.55
2527.10	2.66	-0.45	32.10	3.56	3.70
2529.55	2.81	+0.33	51.90	3.64	3.70
2533.63	2.66	+0.35	48.60	3.33	...
2555.07	2.84	-0.81	12.30	3.44	3.60
2555.45	2.86	-0.83	11.30	3.43	3.60
2559.77	3.23	-0.72	9.30	3.59	3.60
2560.28	3.20	-0.16	3.60
2562.54	0.99	+0.02	105.30	3.50	3.65
2563.48	1.04	-0.23	94.60	3.64	3.70
2566.62	2.81	-1.07	6.60	3.34	3.55
2566.91	1.08	-0.64	3.70
2582.58	1.08	-0.45	77.50	3.52	3.65

TABLE 1 — *Continued*

λ (Å)	χ (eV)	$\log gf$	W (mÅ)	$\log \epsilon_W$	$\log \epsilon_{syn}$
2590.55	2.70	-1.32	7.20	3.52	3.60
2591.54	1.04	-0.46	80.40	3.56	3.65
2592.78	4.08	+0.65	18.20	3.44	3.50
2608.85	2.81	-1.39	7.80	3.73	3.70
2610.63	0.05	+0.92	3.70
2620.17	2.84	-1.15	3.65
2620.70	2.83	-0.55	3.60
2621.67	0.12	-0.94	110.30	3.63	3.70
2626.50	2.86	-0.67	12.60	3.30	3.50
2637.64	3.34	-0.56	6.80	3.37	...
2652.57	3.27	-1.43	2.50	3.69	...
2664.66	3.39	+0.31	29.90	3.43	3.55
2684.75	3.81	+0.23	13.00	3.38	3.60
2721.81	3.15	-1.25	4.20	3.63	3.70
2732.45	0.23	-2.96	39.70	3.68	3.70
2769.36	3.15	-0.48	18.20	3.60	3.60
2917.47	1.04	-2.85	3.65
2965.41	3.42	-2.24	3.65

TABLE 2
ABUNDANCES AND UPPER LIMITS

Species	λ (Å)	χ (eV)	$\log gf$	$\log \epsilon (X)$	Ref.
Be I	2348.61	0.000	+0.140	< -2.30	1
B I	2496.77	0.000	-0.800	< -0.70	1
B I	2497.72	0.002	-0.500	< -0.70	1
C I	2478.56	2.682	-1.110	+5.80 ^a	1
C I	2967.21	0.005	-6.800	+5.75 ^a	1
Sc II	2552.35	0.022	+0.030	-0.44	2
Ti II	2524.64	0.122	-1.320	+1.42	3
Ti II	2525.60	0.151	-0.570	+1.44	3
Ti II	2531.25	0.135	-0.670	+1.48	3
Ti II	2534.62	0.122	-0.930	+1.44	3
Ti II	2841.93	0.607	-0.590	+1.35	3
Ti II	2888.93	0.574	-1.360	+1.49	3
Ti II	2891.06	0.607	-1.140	+1.44	3
Ti II	3058.09	1.180	-0.420	+1.42	3
Cr II	2740.10	1.506	-1.090	+1.62	4
Cr II	2751.87	1.525	-0.290	+1.72	4
Cr II	2757.72	1.506	-0.360	+1.66	4
Cr II	2762.59	1.525	+0.050	+1.68	4
Cr II	2766.54	1.549	+0.320	+1.66	4
Mn II	2576.11	0.000	+0.400	+1.00 ^a	5
Mn II	2605.68	0.000	+0.136	+1.00 ^a	5
Mn II	2933.05	1.175	-0.102	+1.00 ^a	5
Mn II	2949.20	1.175	+0.253	+0.90 ^a	5
Ni I	2289.99	0.000	+0.060	+2.24	6
Ni I	2293.12	0.109	-0.970	+2.25	6
Ni I	2312.34	0.165	+0.410	+2.48	6
Ni I	2325.80	0.165	+0.400	+2.23	6
Ni I	2346.63	0.165	-0.840	+2.33	6
Ni I	2356.87	0.025	-1.510	+2.23	6
Ni I	2360.64	0.275	-1.080	+2.24	6
Ni I	2376.02	0.109	-1.700	+2.36	6
Ni I	2386.59	0.109	-1.180	+2.28	6
Ni I	2419.31	0.165	-1.050	+2.27	6
Ni I	2821.29	0.025	-1.410	+2.37	6
Ni I	2943.91	0.025	-1.170	+2.34	6
Ni I	2992.59	0.025	-1.220	+2.48	6
Ni I	3003.62	0.109	-0.320	+2.17	6
Ni I	3012.00	0.423	+0.000	+2.23	6
Ni I	3031.87	0.000	-1.810	+2.46	6
Ni I	3037.93	0.025	-0.520	+2.40	6
Ni I	3050.82	0.025	-0.100	+2.33	6
Ni I	3054.31	0.109	-0.600	+2.39	6
Ni II	2278.77	1.680	+0.190	+2.21	7
Ni II	2297.14	1.254	-0.070	+2.27	7
Ni II	2297.49	1.322	-0.330	+2.19	7
Ni II	2356.40	1.859	-0.830	+2.29	7
Ni II	2387.76	1.680	-1.070	+2.32	7

TABLE 2 — *Continued*

Species	λ (Å)	χ (eV)	$\log gf$	$\log \epsilon (X)$	Ref.
Ni II	2394.52	1.680	+0.170	+2.09	7
Ni II	2416.14	1.859	+0.130	+2.20	7
Ni II	2437.89	1.680	-0.330	+2.13	7
Ge I	2651.17	0.175	+0.020	< -0.80	8
Ge I	2691.34	0.069	-0.700	< -0.00	8
Ge I	3039.07	0.883	+0.070	< -0.05	8
Zr II	2567.64	0.000	-0.170	< -1.11	9
Zr II	2699.60	0.039	-0.660	< -0.40	10
Zr II	2700.14	0.095	-0.080	< -1.03	9
Zr II	2732.72	0.095	-0.490	< -0.45	9
Zr II	2758.81	0.000	-0.560	< -0.46	9
Zr II	2915.99	0.466	-0.500	< -0.38	9
Zr II	3054.84	1.010	+0.080	< -0.16	10
Nb II	2950.88	0.510	+0.240	< -0.77	11
Nb II	3028.44	0.440	-0.200	< -0.51	11
Mo II	2871.51	1.538	+0.060	< -0.29	12
Cd I	2288.02	0.000	+0.150	< -1.79	13
Te I	2385.79	0.589	-0.810	< -0.05	14
Ce II	3063.00	0.900	+0.400	< -0.51	15
Nd II	3014.17	0.200	-0.660	< -0.01	16
Eu II	2906.67	0.000	-0.350	< -1.46	16
Gd II	3010.13	0.000	+0.190	< -1.21	17
Yb II	2891.39	0.000	-1.169	< -1.75	16
Lu II	2615.43	0.000	-0.270	< -2.16	18
Hf II	2641.41	1.036	+0.570	< -1.11	19
Hf II	2820.23	0.380	-0.140	< -1.31	19
Hf II	2929.64	0.000	-0.940	< -1.02	19
Os I	3058.66	0.000	-0.410	< -0.30	20
Os II	2282.28	0.000	-0.050	< -0.90	20
Pt I	2659.45	0.000	-0.030	< -1.40	21
Pt I	2929.79	0.000	-0.700	< -0.66	21
Pb I	2833.05	0.000	-0.500	< -0.23	22

REFERENCES. — (1) Kramida et al. (2013); (2) Lawler & Dakin (1989); (3) Wood et al. (2013); (4) Bergeson & Lawler (1993); (5) Den Hartog et al. (2011); (6) Wood et al. (2014); (7) Fedchak & Lawler (1999); (8) Fuhr & Wiese (2009); (9) Ljung et al. (2006); (10) Malcheva et al. (2006); (11) Nilsson & Ivarsson (2008); (12) Sikström et al. (2001); (13) Morton (2000); (14) Roederer et al. (2012a); (15) Biémont et al. (1999); (16) Kurucz & Bell (1995); (17) Den Hartog et al. (2006); (18) Roederer et al. (2010a); (19) Lawler et al. (2007); (20) Quinet et al. (2006); (21) Den Hartog et al. (2005); (22) Biémont et al. (2000), using hfs presented in Appendix C of Roederer et al. (2012b).

^a Synthesis

TABLE 3
FINAL NUV LTE ABUNDANCES OF BD+44°493

Species	$\log \epsilon_{\odot}(X)$	$\log \epsilon(X)$	$[X/Fe]$	σ	N
Be I	1.38	< -2.30	< +0.20	...	1
B I	2.70	< -0.70	< +0.48	...	2
C I	8.43	5.78	+1.23	0.20	2
OH	8.69	6.35	+1.54	0.20	11
Sc II	3.15	-0.44	+0.29	0.10	1
Ti II	4.95	1.43	+0.36	0.02	8
Cr II	5.64	1.67	-0.09	0.02	5
Mn II	5.43	0.97	-0.58	0.03	4
Fe I	7.50	3.62	-3.88 ^a	0.01	98
Fe II	7.50	3.63	-3.87 ^a	0.01	53
Ni I	6.22	2.32	-0.02	0.02	19
Ni II	6.22	2.21	-0.13	0.03	8
Ge I	3.65	< -0.80	< -0.57	...	3
Zr II	2.58	< -1.11	< +0.18	...	7
Nb II	1.46	< -0.77	< +1.65	...	2
Mo II	1.88	< -0.29	< +1.71	...	1
Cd I	1.71	< -1.79	< +0.38	...	1
Te I	2.18	< -0.05	< +1.65	...	1
Ce II	1.58	< -0.51	< +1.79	...	1
Nd II	1.42	< -0.01	< +2.45	...	1
Eu II	0.52	< -1.46	< +1.90	...	1
Gd II	1.07	< -1.21	< +1.60	...	1
Yb II	0.84	< -1.75	< +1.29	...	1
Hf II	0.85	< -1.31	< +0.00	...	1
Lu II	0.10	< -2.16	< +1.62	...	1
Hf II	0.85	< -1.31	< +1.72	...	3
Os I	1.40	< -0.30	< +2.18	...	1
Os II	1.40	< -0.90	< +1.58	...	1
Pt I	1.62	< -1.40	< +0.86	...	2
Pb I	1.75	< -0.23	< +1.90	...	1

^a $[Fe\ I/H]$ and $[Fe\ II/H]$ values

TABLE 4
SYSTEMATIC ABUNDANCE UNCERTAINTIES

Species	ΔT_{eff} +150 K	$\Delta \log g$ +0.5 dex	Δv_{micro} +0.3 km/s	σ_{tot}
Sc II	-0.10	-0.17	+0.02	0.20
Ti II	-0.09	-0.17	+0.04	0.20
Cr II	-0.07	-0.16	+0.11	0.21
Mn II	-0.12	-0.06	+0.13	0.19
Fe I	-0.18	+0.02	+0.06	0.19
Fe II	-0.05	-0.15	+0.05	0.17
Ni I	-0.20	+0.02	+0.09	0.22
Ni II	-0.06	-0.17	+0.14	0.23